Standing-Wave Design of Tandem SMB for Linear Multicomponent Systems

Benjamin J. Hritzko and Yi Xie
School of Chemical Engineering, Purdue University, West Lafayette, IN 47907

Robert J. Wooley
National Renewable Energy Laboratory, Golden, CO 80401

Nien-Hwa L. Wang
School of Chemical Engineering, Purdue University, West Lafayette, IN 47907

The standing-wave design was extended to achieve any desired split of mixtures containing three or more components in a single-ring and a tandem two-ring simulated moving bed (SMB). Mass-transfer effects were considered in the design for nonideal systems. The separation of a four-component mixture of glucose, xylose, acetic acid and sulfuric acid was chosen to illustrate the design method. Rate-model simulations confirmed that the standing-wave design method could guarantee high purity and high yield. If all the components in a ternary mixture need to be recovered with high purity and high yield, the easier separation should be performed in the first ring of a tandem SMB to achieve the lowest desorbent consumption and the highest product concentration. If only the intermediate component needs to be recovered in high purity, one of the impurities should be allowed to distribute between the two product ports in the first ring to achieve a lower desorbent consumption and a higher product concentration. These strategies also apply to the separation of a mixture containing more than three components.

Introduction

A major focus of simulated moving-bed (SMB) technology today is in the area of binary separations, often for the resolution of enantiomers for pharmaceuticals and fine chemicals (Juza et al., 2000; Schulte and Strube, 2001). Companies such as Novasep, Knauer, and Mitsubishi Chemicals have capitalized on the growth of the SMB technology by offering separation equipment for the pharmaceutical and fine chemical industries (Blehaut and Nicoud, 1998). UOP and US Filter, among others, offer equipment for low-pressure applications. Some mixtures that can be separated through chromatography have more than two components. SMB processes can be used to separate such mixtures as well. An early example was the UOP Parex process for the recovery of *p*-xylene from a mixture that included *o*-xylene, *m*-xylene, and ethyl benzene (Broughton et al., 1970). In the Parex process, the adsorbent was chosen so that the desired product was the highest-affinity component in the mixture. In general, such an adsorbent is not always available, and it may be necessary to recover a product that has an intermediate affinity.

A major goal of this article is to develop a systematic method for the design of an SMB process for the recovery of a single product or a group of products with intermediate affinities from a multicomponent solution. The treatment in the present article is restricted to linear systems. Examples of SMB units operated under linear conditions include sugar purification (Ching et al., 1991; Wooley et al., 1998) and protein desalination (Hashimoto et al., 1988). The rigorous modeling and design procedure outlined in this article can have a

Correspondence concerning this article should be addressed to N.-H. L. Wang.
Current address of B. J. Hritzko: Pfizer Inc., Groton, CT 06340.
Current address of R. J. Wooley: Cargill Dow, Minnetonka, MN 55345.

significant impact on the yield and cost of large-scale purification.

The conventional four-zone SMB for binary fractionation is the starting point of this study. In such a process, each zone is made up of one or more packed columns, and all of the columns are connected in a circuit. Usually there are two inlet ports and two outlet ports. Through periodic port switching in the direction of fluid flow, the solid sorbent can effectively move in a countercurrent direction with respect to a fluid phase containing the solutes to be separated. When the SMB operating conditions properly account for the migration rate of each component within the bed, two pure products can be withdrawn: a raffinate, which contains the less-retained component(s), and an extract, which contains the more-retained component(s).

Previous researchers have separated multicomponent mixtures into two fractions using a four-zone SMB (Broughton, 1970; Storti et al., 1989; Hatanaka and Ishida, 1992; Hashimoto et al., 1993; Mazzotti et al., 1994, 1996a; Tonkovich and Carr, 1996; Migliorini et al., 2000) or a five-zone SMB (Hotier and Balannec, 1991; Navarro et al., 1997). Others have developed nine-zone parallel SMB units to achieve continuous fractionation of a ternary mixture (Kishihara et al., 1992; Wooley et al., 1998). Ando et al. (1990) and Masuda et al. (1993) proposed to separate a multicomponent mixture into three or more fractions using semicontinuous processes, which consist of two or more steps. Mata and Rodrigues (2001) developed rate models for such processes and analyzed the effects of operating conditions and mass-transfer rates on the performance of such processes. More recently, Nicolaos et al. (2001a,b) have presented strategies for the continuous fractionation of ternary mixtures under ideal conditions for linear and Langmuir-type systems.

In this study, the emphasis is on *tandem* processes, in which two or more SMB units are linked in series. For tandem processes, the desired product plus some unresolved impurities from the first SMB unit are sent to the second unit to obtain a purified center cut.

Finding the optimal zone flow rates and the port switching time is often the major challenge in designing an SMB. Dünnebier et al. (2000) presented a thorough review of the current design approaches. Rhee et al. (1970, 1971) proposed general equations for solute migration in a one-zone, continuous moving bed (CMB) system in the absence of mass-transfer resistances (defined as an "ideal" system in this article). Storti et al. (1989) took into account different flow rates in the different zones of a countercurrent separation process for both linear and nonlinear isotherm systems in the absence of mass-transfer resistance. This concept, when applied to countercurrent chromatography processes, led to the "triangle theory" (Storti et al., 1993), which was named for the triangular region bounding the solution space. This idea was applied to many other SMB separations (Storti et al., 1995; Mazzotti et al., 1994, 1996a,b, 1997; Francotte et al., 1998; Chiang, 1998a,b). Other investigators have also applied linear theory to the design of ideal SMB systems (Zhong and Guiochon, 1996). The SMB design obtained from the triangle theory is typically represented by a two-dimensional plot of the quantities m_2 and m_3, which are dimensionless liquid–solid flow ratios in the zones surrounding the feed port. The infinite set of pairs (m_2, m_3) allowing complete separation and positive feed rate forms a triangle region in the m_2-m_3 plane. In a linear-uptake system operated under ideal conditions, the standing-wave solution is the vertex of the triangle region.

When mass-transfer resistances are significant (defined here as nonideal), the triangular region of solutions shrinks, but still makes up an infinite set in the m_2-m_3 plane (Azevedo and Rodrigues, 1999; Migliorini et al., 1999; Biressi et al., 2000). Similar results are obtained using a "separation volume analysis" of zones I, II, and III (Azevedo and Rodrigues, 1999, 2001). The standing-wave design method can be used to pinpoint a single solution within this reduced set (Ma and Wang, 1997). The standing-wave approach allowed a quick determination of the optimal SMB operating conditions for the separation of two sugars; later, it was applied to SMB processes for the separation of phenylalanine and tryptophan (Wu et al., 1998b) and for the purification of paclitaxel (Wu et al., 1999). Xie et al. (2000) showed that the standing-wave concept can be applied to nonideal systems even when detailed mass-transfer parameters are unavailable. Mallmann et al. (1998) applied the standing-wave design to a binary, nonlinear system. The standing-wave design method is developed in this study for multicomponent separation and used to quickly find optimal separation strategies for multicomponent mixtures.

The separation of a four-component mixture of glucose, xylose, acetic acid, and sulfuric acid was chosen as an example to illustrate the design method. This separation is a key step in a multistep process for converting biomass into ethanol, which is under development at the National Renewable Energy Laboratory. Biomass can be hydrolyzed by sulfuric acid into sugars (mostly xylose and glucose), which need to be separated from the reactant, sulfuric acid, and a byproduct, acetic acid. The recovered sugars can be fermented into ethanol as an alternative fuel or into other fine chemicals. SMB separation has a higher degree of sulfuric acid removal than an alternative precipitation process. In addition, acetic acid and many other minor impurities, which inhibit ethanol fermentation, are also removed (Wooley et al., 1998). Efficient separation of the sugars from the acids will have a major impact on the cost of ethanol and other fine chemicals produced from biomass.

The objectives of this article are summarized below.

(1) Extend the standing-wave analysis for binary mixtures to mixtures with three or more components for both ideal and nonideal systems.

(2) Develop an efficient design method based on the standing-wave approach to split a mixture of three or more components into two fractions in a four-zone SMB.

(3) Validate a detailed SMB rate model (VERSE) and model parameters with experimental data from a pilot SMB operation.

(4) Use simulations based on the validated rate model and model parameters to show that for various splitting strategies, the standing-wave design can guarantee high purity and high yield for nonideal systems.

(5) Apply the standing-wave design to a mixture with three or more components to identify the optimal splitting sequence in a tandem SMB process for the recovery of a component or a group of components with intermediate affinities.

In this study the standing-wave concept is applied to the design of the SMB zone flow rates and the switching time for a specific system, but the approach can be applied to other

linear systems with significant mass-transfer effects (or "nonideal" systems). First, a detailed rate model and model parameters are validated through a comparison of simulation results to experimental data from single-column experiments and a preliminary SMB experiment. Afterward, standing-wave designs are verified with simulations. The zone flow rates, port switching time, and splitting sequence are the key design parameters in this study. It will be shown that the standing-wave design equations for multicomponent separation can be used to find the operating parameters that ensure desired purity and yield for a tandem SMB process. A method for finding the approximate column concentration profiles will be introduced for nonideal systems and will be shown to give conservative estimates of product purities. Splitting strategies are shown to have a major impact on solvent consumption and product dilution for multicomponent separation.

Theory

A major challenge in developing an SMB process is to determine the zone flow rates, zone lengths, and port movement velocity that can guarantee high purity and high yield. This is defined as the "design" problem here. The standing-wave design equations for the separation of a binary mixture were developed in previous articles (Ma and Wang, 1997; Mallmann et al., 1998). The key idea is to consider a limiting case, that is, a CMB system without any mass-transfer effects (or an ideal CMB). The performance of an SMB can approach that of a CMB if a large number of openings are present in the column circuit to allow the four inlet and outlet ports to move almost continuously along the circuit. One can choose the flow rate in each zone, so that the key concentration wave (boundary of a solute band) in each zone migrates at the same speed as the port movement speed. As a result, all band boundaries (or waves) remain "standing" with respect to the ports. As such, the concentration profiles are stable, the compositions of the products remain constant, and high purity and high yield can be achieved. In SMB, only a finite number of ports are present and the ports move periodically. However, as long as the migration speed of the key wave in each zone matches the time-averaged port speed, the time-averaged product concentrations remain constant at cyclic steady state.

Splitting strategies for three-component and N-component mixtures

A four-zone SMB can achieve a binary split of a multicomponent mixture. Two SMBs can be operated in series to recover a single component or a group of components from a multicomponent mixture. Many different splitting strategies can be used. An example for the recovery of a middle component from a ternary mixture is shown in Table 1a. In the first strategy (S1), component 1 (the lowest affinity component) is split from 2 and 3 (the highest affinity component) in the first SMB (first ring or ring A), and the extract product (which contains the unresolved components 2 and 3) is fed to a second SMB (second ring or ring B), in which components 2 and 3 are separated. In an alternative strategy S2, component 3 is split from 1 and 2 in the first ring, and 1 is split from 2 in the second ring.

In some cases, it is not necessary to obtain every component in high purity and high yield. In fact, when only a middle product is required in high purity and high yield, it may be advantageous to allow one or more components to distribute throughout the entire four-zone SMB unit. For example, in Strategy 3 (S3 in Table 1), components 2 and 3 are separated from component 1 in the first ring, so component 1 should be kept away from the extract and collected in the raffinate; however, if components 1 and 3 are not required in high purity, then component 3 should be allowed to distribute or *wrap around* (that is, to migrate from zone I into zone IV) and be recovered with component 1 in the raffinate. Analogously, in Strategy 4, component 1 is allowed to wrap around so that it is withdrawn from both the raffinate and the extract in the first ring.

Extension of the splitting strategies to a mixture of N components is straightforward. Consider a system of N components numbered according to their affinities ($1, \ldots, j_1-1, j_1, \ldots, j_M, j_M+1, \ldots, N$), where component 1 has the lowest affinity, and N has the highest affinity ($M = 1, 2, \ldots$). Any intermediate component(s) (j_1 through j_M) in a mixture of N components can be recovered by two sequential splitting in a

Table 1. Splitting Strategies to Recover a Middle Component or a Group of Components from a Multicomponent Mixture with a Tandem SMB

	1st Ring (Ring A)		2nd Ring (Ring B)	
	Component No.		Component No.	
Strategy	Raffinate	Extract	Raffinate	Extract
	(a) Recovery of Component 2 from Three Components			
S1	1	2 3	2	3
S2	1 2	3	1	2
S3	3 1	2 3	2	3
S4	1 2	3 1	1	2
	(b) Recovery of Component(s) j_1 through j_M ($M = 1, 2, 3\ldots$) from N Components*			
S1	$1, \ldots, j_1-1$	$j_1, \ldots, j_M, j_M+1, \ldots, N$	$j_1, \ldots, j_M$	$j_M+1, \ldots, N$
S2	$1, \ldots, j_1-1, \ldots, j_M$	$j_M+1, \ldots, N$	$1, \ldots, j_1-1$	$j_1, \ldots, j_M$
S3	$1, \ldots, j_1-1, j_M+1, \ldots, N$	$j_1, \ldots, j_M, j_M+1, \ldots, N$	$j_1, \ldots, j_M$	$j_M+1, \ldots, N$
S4	$1, \ldots, j_1-1, j_1, \ldots, j_M$	$1, \ldots, j_1-1, j_M+1, \ldots, N$	$1, \ldots, j_1-1$	$j_1, \ldots, j_M$

*N-Components mixture consists of component $1, 2, \ldots, j_1-1, j_1, \ldots, j_M, j_M+1, \ldots, N$.

tandem SMB using one of the four strategies (Table 1b). As shown later in the standing-wave analysis, the different splitting strategies have a different solvent requirement and product dilution.

Standing-wave design equations for ideal systems for separating a mixture with three or more components

Standing-wave analysis can ensure complete separation of any component or a group of components from the mixture using any of the splitting strategies. The key is the proper choice of a standing-wave in each zone (Table 2). An example of S2 is shown in Figure 1 for splitting an N component mixture into two fractions such that components 1 through j_M are recovered in the raffinate and components j_M+1 through N are recovered in the extract. To achieve a complete binary split, the desorption waves of N and j_M are standing in zone I and zone II, respectively, and the adsorption waves of j_M+1 and 1 are standing in zone III and zone IV, respectively (Figure 1a).

In an ideal system (without mass-transfer resistance), the standing waves can be achieved if the velocity, $u_{w,i}$, of a specific wave in each zone (indicated by an arrow in Figure 1) equals the port movement velocity (ν). For the example shown in Figure 1 (S2)

$$u^{\mathrm{I}}_{w,N} = \nu \quad \text{desorption wave of } N \text{ in zone I} \tag{1}$$

$$u^{\mathrm{II}}_{w,j_M} = \nu \quad \text{desorption wave of } j_M \text{ in zone II} \tag{2}$$

$$u^{\mathrm{III}}_{w,j_M+1} = \nu \quad \text{adsorption wave of } j_M+1 \text{ in zone III} \tag{3}$$

$$u^{\mathrm{IV}}_{w,1} = \nu \quad \text{adsorption wave of 1 in zone IV} \tag{4}$$

For an ideal linear isotherm system,

$$u_{w,i} = \frac{u_0}{1+P\delta_i} \tag{5}$$

where $P \equiv (1-\epsilon_b)/\epsilon_b$ is the mobile-phase/particle-phase volume ratio, ϵ_b is the interparticle void fraction, u_0 is the interstitial linear velocity, and δ_i is the retention factor of solute i

$$\delta_i = K_{e,i}\epsilon_p + (1-\epsilon_p)a_i \tag{6}$$

where $K_{e,i}$ is the size-exclusion factor, ϵ_p is the particle void fraction, and a_i is the low-concentration partition coefficient on a solid-volume basis. According to Eqs. 1 to 4, the interstitial velocity in each zone is related to ν as follows:

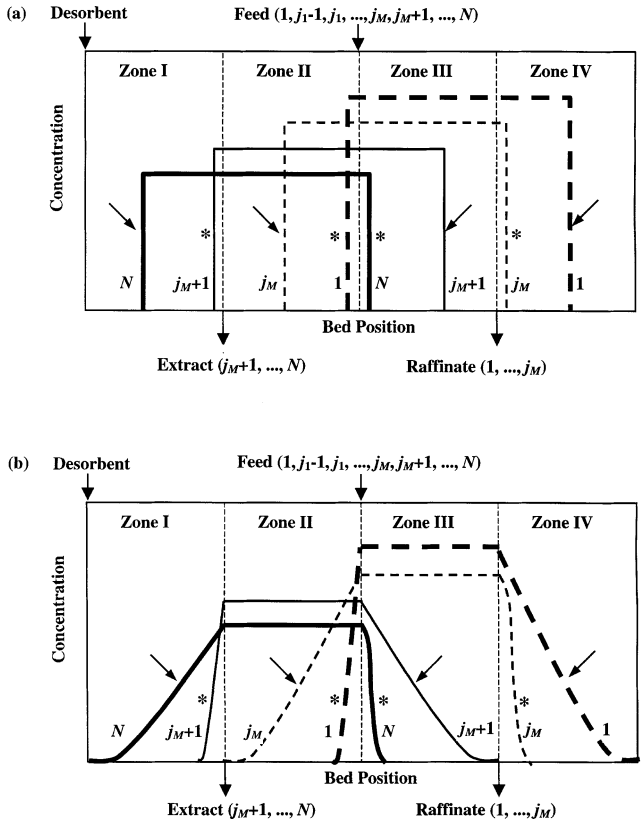

Figure 1. Standing-wave approach for separating N components into two groups of components, 1 through j_M in the raffinate and j_M+1 through N in the extract.

(a) Ideal system. (b) Nonideal system. Angled arrows point to waves that are held standing within a given zone (zone I, N; zone II, j_M; zone III, j_M+1; zone IV, 1). Asterisks point to pinched waves.

Table 2. Standing Waves for Various Splitting Strategies

	Standing Waves							
	1st Ring (Ring A)				2nd Ring (Ring B)			
Strategy	Zone I	Zone II	Zone III	Zone IV	Zone I	Zone II	Zone III	Zone IV
	(a) Recovery of Component 2 from Three Components							
S1	3^*	1^*	2^{**}	1^{**}	3^*	2^*	3^{**}	2^{**}
S2	3^*	2^*	3^{**}	1^{**}	2^*	1^*	2^{**}	1^{**}
S3	2^*	1^*	2^{**}	1^{**}	3^*	2^*	3^{**}	2^{**}
S4	3^*	2^*	3^{**}	2^{**}	2^*	1^*	2^{**}	1^{**}
	(b) Recovery of Component(s) j_1 Through j_M ($M=1, 2, 3, \ldots$) from N Components							
S1	N^*	j_1-1^*	j_1^{**}	1^{**}	N^*	$j_M{}^*$	j_M+1^{**}	j_1^{**}
S2	N^*	$j_M{}^*$	j_M+1^{**}	1^{**}	$j_M{}^*$	j_1-1^*	j_1^{**}	1^{**}
S3	$j_M{}^*$	j_1-1^*	j_1^{**}	1^{**}	N^*	$j_M{}^*$	j_M+1^{**}	j_1^{**}
S4	N^*	$j_M{}^*$	j_M+1^{**}	j_1^{**}	$j_M{}^*$	j_1-1^*	j_1^{**}	1^{**}

*Desorption wave.
**Adsorption wave.

$$u_0^{\mathrm{I}} = (1 + P\delta_N)\,\nu \tag{7}$$

$$u_0^{\mathrm{II}} = (1 + P\delta_{j_M})\,\nu \tag{8}$$

$$u_0^{\mathrm{III}} = (1 + P\delta_{j_M+1})\,\nu \tag{9}$$

$$u_0^{\mathrm{IV}} = (1 + P\delta_1)\,\nu \tag{10}$$

For an ideal system, 100% purity and 100% yield can be achieved at any feed flow rate, F, if the standing-wave conditions in Eqs. 7 to 10 are met. F is related to the difference between u_0^{III} and u_0^{II}

$$F = S\epsilon_b\left(u_0^{\mathrm{III}} - u_0^{\mathrm{II}}\right) \tag{11}$$

$$F = S\epsilon_b P\left(\delta_{j_M+1} - \delta_{j_M}\right)\nu \tag{12}$$

Therefore, the port movement velocity, ν, is related to F

$$\nu = \frac{F}{SP\epsilon_b\left(\delta_{j_M+1} - \delta_{j_M}\right)} \tag{13}$$

In converting from a continuous moving port system to an equivalent SMB it is assumed that the periodic switching of the ports approximates the continuous port movement, that is, $\nu = L_c/t_s$, where L_c is the single-column length and t_s is the switching time. In conventional CMB terminology the liquid-phase velocity, u_0^{CMB}, is reported relative to the opposing solid-phase velocity, whereas in SMB terminology it is customary to use a stationary frame of reference; thus, $u_0^{SMB} \equiv u_0^{CMB} + \nu$. Unless otherwise noted, all of the interstitial velocities in this work are based on an SMB.

In Figure 1a, some waves are migrating at a slower speed or a higher speed than the average port velocity in an ideal system. In zone I, for example, the desorption wave of N is standing, whereas the desorption waves of $j_M + 1$ through $N - 1$ are migrating at higher speeds than the port velocity. These waves shift downstream toward the extract port. They cannot continue to shift downstream into zone II because under the flow rate of zone II, the waves are migrating at a lower speed than the average port velocity. As a result, these waves are stuck or *pinched* between the two zones. These waves are defined here as the *pinched waves*. Similarly, the desorption waves of 1 through $j_M - 1$ in zone II, the adsorption waves of $j_M + 2$ through N in zone III, and the adsorption waves of 2 through j_M in zone IV are pinched waves.

Standing-wave equations for other splitting strategies S1, S3, and S4 can be derived according to the standing waves listed in Table 2. A group of components (j_1 through j_M) can also be recovered using two sequential splits in a tandem SMB. The standing waves for such separations are listed in Table 2b.

Standing-wave design equations for nonideal systems for separating a mixture with three or more components

For a linear, nonideal system, Ma and Wang (1997) proposed to modify the interstitial velocities for an ideal system to ensure high purity and high yield in a nonideal system. The key idea is to increase the linear velocities in zone I and zone II such that the two desorption waves migrate slightly faster than the ports. This adjustment shifts the centers of the desorption waves downstream relative to the ports. Similarly, the linear velocities in zone III and zone IV are reduced such that the center of the adsorption waves are shifted upstream relative to the ports.

The zone velocity adjustments, which are needed to counter mass-transfer spreading, are functions of mass-transfer parameters, zone lengths, isotherm parameters, and a decay factor (β) that is related to purity. Detailed analysis and equations for the separation of a binary mixture in a four-zone SMB have been reported previously (Ma and Wang, 1997). These adjustments have been proven effective experimentally (Wu et al., 1998b; Xie et al., 2000).

Because the solutes in linear systems are noninteracting, the correction terms can be applied to multicomponent linear systems. Equations 7 to 10 for the first ring of splitting strategy S2 can be modified as follows

$$u_0^{\mathrm{I}} = (1 + P\delta_N)\,\nu + \Delta_N^{\mathrm{I}} \tag{14}$$

$$u_0^{\mathrm{II}} = (1 + P\delta_{j_M})\,\nu + \Delta_{j_M}^{\mathrm{II}} \tag{15}$$

$$u_0^{\mathrm{III}} = (1 + P\delta_{j_M+1})\,\nu - \Delta_{j_M+1}^{\mathrm{III}} \tag{16}$$

$$u_0^{\mathrm{IV}} = (1 + P\delta_1)\,\nu - \Delta_1^{\mathrm{IV}} \tag{17}$$

The mass-transfer correction terms are defined as

$$\Delta_i^m \equiv \frac{\beta_i^m}{L^m}\left(E_{b,i}^m + \frac{P\delta_i^2\nu^2}{K_{f,i}^m}\right) \tag{18}$$

The superscript m designates the zone number, the subscript i designates the component, $E_{b,i}^m$ is the axial dispersion coefficient of component i in zone m, and L^m is the length of zone m. The lumped mass-transfer coefficient, $K_{f,i}^m$, for component i in zone m can be estimated from pulse data or calculated from the following equation

$$\frac{1}{K_{f,i}^m} = \frac{R_p^2}{15K_{e,i}\epsilon_p D_{p,i}} + \frac{R_p}{3k_{f,i}^m} \tag{19}$$

This parameter lumps the effects of film mass transfer and pore diffusion into a single term (Ruthven, 1984). The parameter β_i^m is the decay factor for the standing wave of component i in zone m. It is defined as follows

$$\beta_i^m \equiv \ln\left(\frac{C_{i,\max}^m}{C_{i,\min}^m}\right) \tag{20}$$

where $C_{i,\max}^m$ represents the time-averaged maximum concentration of component i in zone m. A method to relate the desired product purity and yield to β_i^m is presented in Appendix A. For a given feed flow rate F, ν is the root of the following equation

$$\left(\frac{P\beta_{j_M+1}^{\mathrm{III}}\delta_{j_M+1}^2}{K_{f,j_M+1}^{\mathrm{III}}L^{\mathrm{III}}} + \frac{P\beta_{j_M}^{\mathrm{II}}\delta_{j_M}^2}{K_{f,j_M}^{\mathrm{II}}L^{\mathrm{II}}}\right)\nu^2 - P\left(\delta_{j_M+1} - \delta_{j_M}\right)\nu + \frac{F}{\epsilon_b S} + \frac{\beta_{j_M+1}^{\mathrm{III}}E_{b,j_M+1}^{\mathrm{III}}}{L^{\mathrm{III}}} + \frac{\beta_{j_M}^{\mathrm{II}}E_{b,j_M}^{\mathrm{II}}}{L^{\mathrm{II}}} = 0 \tag{21}$$

Equation 21 arises from a mass balance at the feed port, at which point the flow rate to zone III equals the flow rate in

zone II plus the feed flow rate. The maximum feed flow rate, F_{max}, for a given configuration can be calculated from the discriminant of the quadratic formula associated with Eq. 21.

Since the mass-transfer parameters E_b and K_f can vary with flow rate, the set of operating parameters (the four zone flow rates and the switching time) are found through iterative calculation of Eqs. 14 to 21. The initial solution set comes from the equations for ideal systems (Eqs. 7 to 11). These operating conditions are used to estimate mass-transfer parameters for each component in each zone, which are in turn used in Eqs. 14 to 17 and 21 to recalculate the zone flow rates and the switching time. The iterative calculation is continued until the flow rates and switching time change by less than 0.01% at each step.

The preceding design equations are also valid in nonadsorbing systems (with $a_i = 0$ for all i in Eq. 6). Within this classification, size-exclusion chromatography can be considered as a special case, where the solutes are separated solely on the basis of differing degrees of exclusion from the particle pores (that is, different values of $K_{e,i}$).

In order to achieve high purity and high yield in a nonideal system, the migration velocities of the waves that correspond to the standing waves in an ideal system were modified slightly according to Eqs. 14 to 17. Under the modified linear zone velocities, the centers of these waves no longer migrate at the same speed as the port. Since the leading and trailing edges of the spread waves remain standing, these waves are still called the standing waves here. The term pinched waves is reserved for the waves that are pinched in the absence of mass-transfer effects.

Solvent consumption and product dilution for different splitting strategies — ideal systems

The standing-wave analysis can help to quickly identify the best splitting strategy for a given separation. In the comparison of these alternative strategies, the standing-wave equations for ideal systems are analyzed first. Desorbent consumption, product dilution, and relative throughput are calculated and compared for each case. In the splitting strategy S1 with a feed flow rate, F_A, an apparent solid movement velocity, ν_A, can be calculated from Eq. 13. Using the differences between the zone flow rates, one can calculate the following inlet and outlet flow rates under standing-wave conditions

$$F_A = PS\epsilon_b\nu_A(\delta_2 - \delta_1) \tag{22}$$

$$D_A = PS\epsilon_b\nu_A(\delta_3 - \delta_1) \tag{23}$$

$$E_A = PS\epsilon_b\nu_A(\delta_3 - \delta_1) \tag{24}$$

where D_A is the desorbent flow rate for ring A and E_A is the extract flow rate. Combining Eqs. 22 and 23 leads to the following relationship

$$D_A = \left(\frac{\delta_3 - \delta_1}{\delta_2 - \delta_1}\right)F_A \tag{25}$$

The extract from ring A is fed into ring B, thus

$$F_B = E_A = PS\epsilon_b\nu_A(\delta_3 - \delta_1) = \left(\frac{\delta_3 - \delta_1}{\delta_2 - \delta_1}\right)F_A \tag{26}$$

It is easy to show that $D_B = F_B$, so that

$$D_B = \left(\frac{\delta_3 - \delta_1}{\delta_2 - \delta_1}\right)F_A \tag{27}$$

and

$$D_{total} = D_A + D_B = 2\left(\frac{\delta_3 - \delta_1}{\delta_2 - \delta_1}\right)F_A \tag{28}$$

The specific throughput is defined as $F/PS\epsilon_b\nu$, which can be calculated from Eq. 22. Product dilution ($C_{2,prod}/C_{2,feed}$) can be derived from the overall balance of component 2 over the two rings. A similar derivation is applied to the other strategies. The final results are summarized in Table 3. The analysis for three-component systems is extended to N-component systems; the standing waves are listed in Table 2 and the final results are listed in Table 4. Detailed analyses on the separation of three-component and N-component mixtures are discussed in the Results section.

Solvent consumption and product dilution for the different splitting strategies — nonideal systems

When mass-transfer resistances are considered, the SMB designs are highly dependent on column size, column configuration, and individual mass-transfer parameters. Taking the splitting strategy S1, one could specify a feed flow rate, F_A, and calculate an apparent solid velocity, ν_A, from Eq. 21. Applying Eqs. 14 to 17 and mass balance at the inlet and outlet ports, one can write the following

$$F_A = S\epsilon_b\left[P\nu_A(\delta_2 - \delta_1) - \Delta_2^{\mathrm{III}A} - \Delta_1^{\mathrm{II}A}\right] \tag{29}$$

$$D_A = S\epsilon_b\left[P\nu_A(\delta_3 - \delta_1) + \Delta_3^{\mathrm{I}A} + \Delta_1^{\mathrm{IV}A}\right] \tag{30}$$

$$E_A = S\epsilon_b\left[P\nu_A(\delta_3 - \delta_1) + \Delta_3^{\mathrm{I}A} - \Delta_1^{\mathrm{II}A}\right] \tag{31}$$

Table 3. Input and Output of Ring A, Solvent Consumption, and Product Concentration in a Tandem SMB with Two SMB Units for an Ideal System: Three Components

Strategy	Ring A (R/E)	Ring B (R/E)	$F_A/\nu_A P\epsilon_b S_A$	$F_B/\nu_A P\epsilon_b S_A$	D_{total}/F	$C_{2,prod}/C_{2,feed}$	Pure Products
S1	1/2,3	2/3	$\delta_2 - \delta_1$	$\delta_3 - \delta_1$	$\frac{2(\delta_3 - \delta_1)}{(\delta_2 - \delta_1)} > 2$	$\frac{(\delta_2 - \delta_1)}{(\delta_3 - \delta_1)} < 1$	1, 2, 3
S2	1,2/3	1/2	$\delta_3 - \delta_2$	$\delta_3 - \delta_1$	$\frac{2(\delta_3 - \delta_1)}{(\delta_3 - \delta_2)} > 2$	$\frac{(\delta_3 - \delta_2)}{(\delta_3 - \delta_1)} < 1$	1, 2, 3
S3	3,1/2,3	2/3	$\delta_2 - \delta_1$	$\delta_2 - \delta_1$	2	1	2
S4	1,2/3,1	1/2	$\delta_3 - \delta_2$	$\delta_3 - \delta_2$	2	1	2

Table 4. Relative Throughput, Solvent Consumption, and Product Concentration in a Tandem SMB with Two SMB Units for an Ideal System: *N* Components

Strategy	$\frac{F_A}{\nu_A P \epsilon_b S_A}$	$\frac{F_B}{\nu_A P \epsilon_b S_A}$	$\frac{D_{\text{total}}}{F_A}$	$\frac{\sum_{k=1}^{M} C_{j_k,\text{product}}}{\sum_{k=1}^{M} C_{j_k,\text{feed}}}$	Pure Products*
S1	$\delta_{j_1}-\delta_{j_1-1}$	$\delta_N-\delta_{j_1-1}$	$\frac{\delta_N-\delta_1}{\delta_{j_1}-\delta_{j_1-1}}+\left(\frac{\delta_N-\delta_{j_1}}{\delta_{j_M+1}-\delta_{j_M}}\right)\left(\frac{\delta_N-\delta_{j_1-1}}{\delta_{j_1}-\delta_{j_1-1}}\right)$	$\left(\frac{\delta_{j_1}-\delta_{j_1-1}}{\delta_N-\delta_{j_1-1}}\right)\left(\frac{\delta_{j_M+1}-\delta_{j_M}}{\delta_{j_M+1}-\delta_{j_1}}\right)$	$j_1, \ldots, j_M$, lower and upper cuts
S2	$\delta_{j_M+1}-\delta_{j_M}$	$\delta_{j_M+1}-\delta_1$	$\frac{\delta_N-\delta_1}{\delta_{j_M+1}-\delta_{j_M}}+\left(\frac{\delta_{j_M}-\delta_1}{\delta_{j_1}-\delta_{j_1-1}}\right)\left(\frac{\delta_{j_M+1}-\delta_1}{\delta_{j_M+1}-\delta_{j_M}}\right)$	$\left(\frac{\delta_{j_M+1}-\delta_{j_M}}{\delta_{j_M+1}-\delta_1}\right)\left(\frac{\delta_{j_1}-\delta_{j_1-1}}{\delta_{j_M}-\delta_{j_1-1}}\right)$	$j_1, \ldots, j_M$, lower and upper cuts
S3	$\delta_{j_1}-\delta_{j_1-1}$	$\delta_{j_M}-\delta_{j_1-1}$	$\frac{\delta_{j_M}-\delta_1}{\delta_{j_1}-\delta_{j_1-1}}+\left(\frac{\delta_N-\delta_{j_1}}{\delta_{j_M+1}-\delta_{j_M}}\right)\left(\frac{\delta_{j_M}-\delta_{j_1-1}}{\delta_{j_1}-\delta_{j1_{-1}}}\right)$	$\left(\frac{\delta_{j_1}-\delta_{j_1-1}}{\delta_{j_M}-\delta_{j_{1-1}}}\right)\left(\frac{\delta_{j_M+1}-\delta_{j_M}}{\delta_{j_M+1}-\delta_{j_1}}\right)$	$j_1, \ldots, j_M$
S4	$\delta_{j_M+1}-\delta_{j_M}$	$\delta_{j_M+1}-\delta_{j_1}$	$\frac{\delta_N-\delta_{j_1}}{\delta_{j_M+1}-\delta_{j_M}}+\left(\frac{\delta_{j_M}-\delta_1}{\delta_{j_1}-\delta_{j_1-1}}\right)\left(\frac{\delta_{j_M+1}-\delta_{j_1}}{\delta_{j_M+1}-\delta_{j_M}}\right)$	$\left(\frac{\delta_{j_M+1}-\delta_{j_M}}{\delta_{j_M+1}-\delta_{j_1}}\right)\left(\frac{\delta_{j_1}-\delta_{j_1-1}}{\delta_{j_M}-\delta_{j_1-1}}\right)$	$j_1, \ldots, j_M$

*Component(s) $j_1, \ldots, j_M$ ($M = 1, 2, \ldots$) are the desired products(s).

The terms Δ_i^m are always positive. Next, the feed flow rate for ring B can be set to E_A and Eq. 21 can be used to calculate the port movement velocity ν_B for the second ring. In this way, one can calculate

$$D_B = S\epsilon_b\left[P\nu_B(\delta_3-\delta_2)+\Delta_3^{\text{I}B}+\Delta_2^{\text{IV}B}\right] \tag{32}$$

The total desorbent consumption is, therefore

$$D_{\text{total}} = S\epsilon_b\left[P\nu_A(\delta_3-\delta_1)+P\nu_B(\delta_3-\delta_2)+\Delta_3^{\text{I}A}+\Delta_1^{\text{IV}A}+\Delta_3^{\text{I}B}+\Delta_2^{\text{IV}B}\right] \tag{33}$$

Explicit solutions of ν_A and ν_B can be easily derived, but are not shown here for brevity. These equations can be solved numerically. The total desorbent consumption for each case is listed in Table 5. Relative throughput and product dilution can be derived similarly as for ideal systems once ν_A and ν_B are known. This analysis is easily extended to an N-component system and the results are presented in Table 6.

It is clear from Table 5 that if all the mass-transfer correction terms Δ_i^m are relatively small compared to the equilibrium terms (containing δ_i) and they are similar in values, D_{total} will be dominated by the equilibrium parameters. In this case, the conclusions about the splitting strategies for nonideal systems are the same as those for ideal systems.

It is theoretically possible (albeit rarely in practice) that the mass-transfer correction terms (Table 5) are in the same order of magnitude or larger than the equilibrium terms. In this case, the choice of splitting strategy will not be determined only by the equilibrium parameters δ_i. One can choose a preliminary splitting strategy based on the ideal analysis, and carry out the standing-wave design for the chosen splitting strategy. In order to find out whether the mass-transfer correction terms are overtaking the equilibrium terms, one can lump the correction terms Δ_i^m with the corresponding equilibrium terms δ_i and treat the sum as an "effective" δ_i or $\delta_{i,\text{effective}}$

$$\delta_{i,\text{effective}} = \delta_i + (\Delta_i^m/P\nu) \quad m = \text{I, II} \tag{34}$$

$$\delta_{i,\text{effective}} = \delta_i - (\Delta_i^m/P\nu) \quad m = \text{III, IV} \tag{35}$$

One can examine the $\delta_{i,\text{effective}}$ values in each zone to see whether the affinity sequence and the rank of the affinity difference remain identical to that of the corresponding ideal system. If they are identical, the best splitting strategy from the ideal analysis holds. If they are not, one should carry out the standing-wave designs for all possible splitting strategies and compare the results to decide the best splitting strategy. It should be kept in mind that the terms Δ_i^m depend on the SMB design and operating parameters (flow rates, step time,

Table 5. Solvent Consumption for the Separation Strategies in Table 1 Considering Mass-Transfer Resistances: Three Components

Strategy	Ring A (R/E)	Ring B (R/E)	D_{total}	High-Purity Products
S1	1/2,3	2/3	$PS\epsilon_b\nu_A(\delta_3-\delta_1)+PS\epsilon_b\nu_B(\delta_3-\delta_2)+\Delta_3^{\text{I}A}+\Delta_1^{\text{IV}A}+\Delta_3^{\text{I}B}+\Delta_2^{\text{IV}B}$	1, 2, 3
S2	1,2/3	1/2	$PS\epsilon_b\nu_A(\delta_3-\delta_1)+PS\epsilon_b\nu_B(\delta_2-\delta_1)+\Delta_3^{\text{I}A}+\Delta_1^{\text{IV}A}+\Delta_2^{\text{I}B}+\Delta_1^{\text{IV}B}$	1, 2, 3
S3	3,1/2,3	2/3	$PS\epsilon_b\nu_A(\delta_2-\delta_1)+PS\epsilon_b\nu_B(\delta_3-\delta_2)+\Delta_2^{\text{I}A}+\Delta_1^{\text{IV}A}+\Delta_3^{\text{I}B}+\Delta_2^{\text{IV}B}$	2
S4	1,2/3,1	1/2	$PS\epsilon_b\nu_A(\delta_3-\delta_2)+PS\epsilon_b\nu_B(\delta_2-\delta_1)+\Delta_3^{\text{I}A}+\Delta_2^{\text{IV}A}+\Delta_2^{\text{I}B}+\Delta_1^{\text{IV}B}$	2

Table 6. Solvent Consumption for Separation Strategies in Table 1 Considering Mass-Transfer Resistances: *N* Components

Strategy	D_{total}	High-Purity Products*
S1	$PS\epsilon_b\nu_A(\delta_N-\delta_1)+PS\epsilon_b\nu_B(\delta_N-\delta_{j_1})+\Delta_N^{\text{I}A}+\Delta_1^{\text{IV}A}+\Delta_N^{\text{I}B}+\Delta_{j_1}^{\text{IV}B}$	$j_1, \ldots, j_M$, lower and upper cuts
S2	$PS\epsilon_b\nu_A(\delta_N-\delta_1)+PS\epsilon_b\nu_B(\delta_{j_M}-\delta_1)+\Delta_N^{\text{I}A}+\Delta_1^{\text{IV}A}+\Delta_{j_M}^{\text{I}B}+\Delta_1^{\text{IV}B}$	$j_1, \ldots, j_M$, lower and upper cuts
S3	$PS\epsilon_b\nu_A(\delta_{j_M}-\delta_1)+PS\epsilon_b\nu_B(\delta_N-\delta_{j_1})+\Delta_{j_M}^{\text{I}A}+\Delta_1^{\text{IV}A}+\Delta_N^{\text{I}B}+\Delta_{j_1}^{\text{IV}B}$	$j_1, \ldots, j_M$
S4	$PS\epsilon_b\nu_A(\delta_N-\delta_{j_1})+PS\epsilon_b\nu_B(\delta_{j_M}-\delta_1)+\Delta_N^{\text{I}A}+\Delta_{j_1}^{\text{IV}A}+\Delta_{j_M}^{\text{I}B}+\Delta_1^{\text{IV}B}$	$j_1, \ldots, j_M$

*Component(s) $j_1, \ldots, j_M$ ($M = 1, 2, \ldots$) are the desired product(s).

and so on). The calculated $\delta_{i,\text{effective}}$ can vary from zone to zone. For this reason, one must examine the $\delta_{i,\text{effective}}$ for all the zones. This approach is tested in the sugar–acid separation example.

Rate model

The standing-wave design method is derived for a continuous moving port system or a true moving-bed system. To check the validity of the method for SMB systems, simulations based on a detailed rate model for SMB (moving port) are used for comparison. Product purity and yield obtained from the simulations are compared with those target values set in the standing-wave design. In this study, the rate model and the simulation program is first validated with data obtained from batch elution and SMB experiments.

For single-column and multiple-column studies, a mathematical model based on pore diffusion is used. The model assumptions, equations, boundary conditions, initial conditions, and a numerical method are shown in Appendix B.

Results and Discussion

Model and parameter validation — single-column tests

Two sets of pulse data (Wooley et al., 1998) were compared with rate model simulations to validate isotherms, mass-transfer parameters, and the applicability of the mathematical model for predicting wave propagation. Wooley et al. (1998) reported the first moments of these four pulses. The partition coefficients were calculated from the first moments, according to the following material balance

$$a_i = \frac{F\left(t_{r,i} - t_{0,i} - t_p/2\right)}{V_c(1-\epsilon_b)\left(1-\epsilon_p\right)} \tag{36}$$

where $t_{r,i}$ is the solute retention time (first moment) and t_p is the time of the pulse injection. The term $t_{0,i}$ is the retention time of a nonadsorbing solute, i, and it is calculated as

$$t_{0,i} = \frac{V_c\left[\epsilon_b + (1-\epsilon_b)K_{e,i}\epsilon_p\right]}{F} \tag{37}$$

Table 7 lists the partition coefficients of the four components in this system.

Values of the Brownian diffusivity in water at 25°C in the literature can be found for sulfuric acid (Cussler, 1997), glucose (Doran, 1995), xylose (Lielmezs et al., 1990), and acetic acid (Cussler, 1997). The pulse tests were carried out at 65°C. The values of the Brownian diffusivities at 25°C were adjusted to 65°C using the Stokes–Einstein equation (Cussler, 1997). The axial dispersion coefficient of each component is calculated from the empirical correlation $E_{b,i} = 0.05u_0$ for pulse simulations (Wooley et al., 1998). The film mass-transfer coefficient, $k_{f,i}$, is calculated from the correlation by Wilson and Geankoplis (1966). The intraparticle diffusivity, $D_{p,i}$,

Table 7. Isotherm and Mass-Transfer Parameters Used in Simulations

Component, i		Sulfuric Acid	Glucose	Xylose	Acetic Acid
Isotherms	$K_{e,i}$	0.24	0.42	0.42	0.42
	$t_{r,i}$ [s]	840	1140	1200	1560
	$t_{0,i}$ [s]	780	900	900	900
	a_i [m³/m³ S.V.]	0.00	0.56	0.64	1.54
	δ_i	0.15	0.47	0.51	0.86
Mass-transfer parameters (SMB)	D_i^{∞} [m²/s]				
	25°C	1.73×10^{-9}	7.73×10^{-10}	7.45×10^{-10}	1.21×10^{-9}
	65°C	4.03×10^{-9}	1.80×10^{-9}	1.73×10^{-9}	2.82×10^{-19}
	$E_{b,i}$ [m²/s]				
	Pulse	$0.05\,u_0$	$0.05\,u_0$	$0.05\,u_0$	$0.05\,u_0$
	SMB	$2.5\,u_0$	$2.5\,u_0$	$2.5\,u_0$	$2.5\,u_0$
	$k_{f,i}$ [m/s]	WG	WG	WG	WG
	$K_{f,i}$ [s⁻¹]	Eq. 19	Eq. 19	Eq. 19	Eq. 19
	$D_{p,i}$ [m²/s]				
	25°C	1.28×10^{-10}	1.65×10^{-10}	2.00×10^{-10}	7.17×10^{-11}
	65°C	3.00×10^{-10}	3.83×10^{-10}	4.50×10^{-10}	1.67×10^{-10}

WG = Wilson and Geankoplis (1966) correlation in each zone.

Table 8. System and Operating Parameters for the SMB Experiment in Figure 2

Parameter	Value
Number of columns	20
Column length	1.0 m
Column inner diameter	0.0337 m
Packing void fraction, ϵ_b	0.39
Particle void fraction, ϵ_p	0.60
Column configuration*	3–4–9–4
Switching time	180.0 s
Feed flow rate	5.55×10^{-7} m^3/s
Desorbent flow rate	1.83×10^{-6} m^3/s
Raffinate flow rate	1.87×10^{-6} m^3/s
Extract flow rate	5.17×10^{-7} m^3/s
Zone I flow rate	3.43×10^{-6} m^3/s
Zone II flow rate	2.92×10^{-6} m^3/s
Zone III flow rate	3.47×10^{-6} m^3/s
Zone IV flow rate	1.60×10^{-6} m^3/s
Sulfuric acid feed concentration	11.32 kg/m^3
Glucose feed concentration	9.58 kg/m^3
Xylose feed concentration	40.70 kg/m^3
Acetic acid feed concentration	16.76 kg/m^3

*Allocation of columns in zones I, II, III, and IV, respectively.

is computed from Eq. 19, and the value of the lumped mass-transfer parameter, $K_{f,i}$, reported by Wooley et al. (1998) for each component 65°C. The mass-transfer parameters are listed in Table 7.

Wooley et al. (1998) showed close agreement between lumped model simulations and the experimental pulse data. Simulations obtained from the detailed pore-diffusion model described in Appendix B have a similar agreement with the pulse data (not shown here for brevity). The results support the validity of the rate model and model parameters, which are validated further with the SMB pilot test.

Model and parameter validation — SMB pilot test

One set of four-zone SMB data from a preliminary experiment was compared to the output of a simulation to validate the isotherm and mass-transfer parameters as well as the port-switching routine in the simulation package. The parameters obtained from the single-column pulse tests were used to design a preliminary four-zone SMB process. The objective of this SMB run was to remove most of the sulfuric acid from the sugars. Acetic acid is allowed to distribute throughout the SMB, as in strategy S3. The operating parameters for this experiment are listed in Table 8. Note that the preliminary design was determined empirically instead of by the standing-wave analysis. The operating conditions in this SMB experiment resulted in a purity and yield of about 90% for the two sugars.

The column concentration profile is shown in Figure 2. The data were taken after eight cycles. The operation was approaching a periodic steady state. To obtain column samples, the system was shut down at the end of the last step (all flows and port rotation was simultaneously and instantaneously stopped). Each column was then drained and the liquid collected was analyzed via HPLC (Biorad Aminex 87H column, with a mobile phase of 0.01 N H_2SO_4). Therefore, the compositions of the samples represent averaged concentrations in each column within the SMB unit.

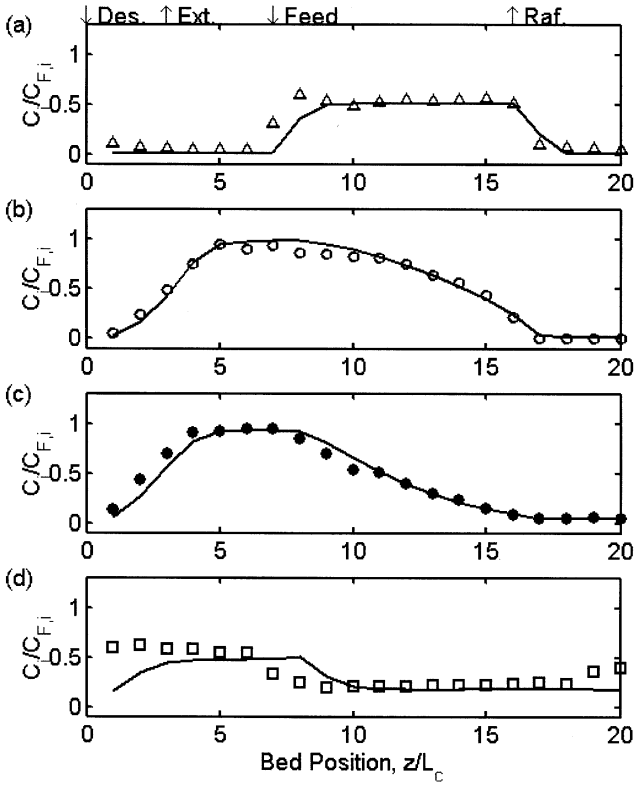

Figure 2. Preliminary SMB experiment for removing sulfuric acid from glucose, xylose, and acetic acid.

All data are taken from the same SMB experiment. Operating parameters are listed in Table 8. (a) Sulfuric acid; (b) glucose; (c) xylose, (d) acetic acid.

The simulated column profiles were also taken at the end of the eighth cycle. The concentrations were then averaged within each column and plotted against the experimental data in Figure 2. In the simulation of the SMB experiment, the isotherm parameters determined from the batch experiments were used. The pulse tests were carried out at 65°C, whereas the SMB pilot test was carried out at room temperature, 25°C. The values of the intraparticle diffusivities were adjusted using the Stokes–Einstein equation (Cussler, 1997). The axial dispersion correlation for the SMB simulations are generated under the assumption that $E^m_{b,i} = 2.5u^m_0$. Wooley et al. (1998) suggested the latter correlation should be used to account for nonideal packing and extracolumn mixing through pumps and valves in the pilot SMB system. The good agreement shown in Figure 2 indicates that the isotherm and mass-transfer parameters used in the simulations are quite accurate except for acetic acid. Apparently, the isotherm parameters of the excluded solute, sulfuric acid, and the two weakly adsorbed sugars at 25°C are similar to those at 65°C. The experimental profile of acetic acid lags behind the simulated profile based on the isotherm at 65°C. This result indicates that the isotherm value of acetic acid at 25°C is larger than that at 65°C.

Wooley et al. (1998) reported additional data for three SMB experimental runs at 65°C from the same system, which was configured as a nine-zone parallel SMB. Close agreement be-

tween the simulations and the data from the SMB runs further confirms that the experimental method is sound and the engineering parameters at 65°C are accurate.

Splitting strategies for three-component and N-component mixtures in ideal systems

For the separation of a ternary mixture, the complete separation strategies S1 and S2 require more desorbent and cause more product dilution than S3 and S4, where one impurity is allowed to distribute in the first ring (Table 3). The desirable qualities of S3 and S4 are achieved at the price of obtaining only one pure product. Strategies S1 and S2 lead to a higher desorbent consumption and a higher degree of product dilution, but three pure products are obtained. It should be emphasized that in choosing between S1 and S2, it is assumed that lower desorbent consumption and lower product dilution are preferred. From Table 3, one can see that if $(\delta_2 - \delta_1) > (\delta_3 - \delta_2)$, then S1 should be chosen over S2 for complete separation, because the desorbent requirement and the product dilution are lower. If $(\delta_3 - \delta_2) > (\delta_2 - \delta_1)$, then S2 should be chosen for the same reason. In other words, the easier separation should be performed in the first ring in order to have the advantages of the least amount of desorbent, the least product dilution, and the highest specific throughput. Strategies S3 and S4 have the same desorbent requirement and no product dilution. For these two cases, an easier split in the first ring gives a higher specific throughput and a lower specific output from the first ring.

With N components some of the conclusions for three-component separation still hold. Both S1 and S2 result in product dilution when $j_M < N$ and $j_1 > 1$. If $j_1 = 1$ or $j_M = N$, then a tandem SMB process is unnecessary, because the desired products can be obtained in a single ring. The desorbent-to-feed ratio and the product dilution are lower for S3 and S4 than for S1 and S2 (Table 4). The impurities that do not need to be recovered in pure form should be distributed in the first ring. Notice that the distributed impurities can have either higher or lower affinities than the product, depending on the case (S3 or S4). There is no difference in the normalized product concentration (either $C_{j_k,\text{product}}/C_{j_k,\text{feed}}$ or $\sum_{k=1}^{M} C_{j_k,\text{product}}/\sum_{k=1}^{M} C_{j_k,\text{feed}}$) between S3 and S4 as shown in Table 4. However, the values of D_{total}/F_A of S3 and S4 can be different. The following conditions can be derived from Table 4. If $(\delta_N - \delta_{j_M}) > (\delta_{j_1} - \delta_1)$, then D_{total}/F_A of S3 is higher than that of S4; if $(\delta_N - \delta_{j_M}) = (\delta_{j_1} - \delta_1)$, then S3 and S4 result in the same D_{total}/F_A; and if $(\delta_N - \delta_{j_M}) < (\delta_{j_1} - \delta_1)$, then D_{total}/F_A of S3 is lower than that of S4. If only one intermediate product needs to be recovered (that is, $j_1 = j_M$), then S3 and S4 have the same D_{total}/F_A. Solvent consumption depends on both the adsorption strengths of the two nearest neighbors of the split and those of the most and the least retained components (Table 4).

In general, the lowest solvent consumption and the highest product concentration can be achieved if the easier separation is done first and the impurities that coelute with the product are distributed in the first ring.

Table 9. Numerical Parameters Used in the Simulations

Parameter	Value
No. of axial elements	1,000
No. of collocation points per element	4
No. of collocation points per particle	2
Absolute tolerance on concentration	0.001 kg/m^3
Relative tolerance on concentration	0.0001
Max. step time in integration	0.1 bed volumes

Standing-wave design methods and splitting strategies for nonideal systems separating glucose and xylose from sulfuric acid and acetic acid

In this example, two 20-column SMB units in series are used to recover glucose and xylose from the four-component sugar–acid mixture. In the design of the SMB processes for the recovery of the two sugars, the four strategies in Table 1b with $N = 4$ and $M = 2$ are used. For each case, the feed to the first SMB has a flow rate of 5.55×10^{-7} m^3/s and a composition as given in Table 8. The column length and zone configuration for each ring in each strategy are kept the same as those of the pilot test. The diameter of the second ring is chosen such that the switching time of the second ring is between 3 and 5 min. Both the standing-wave design without considering -transfer effects (ideal design) and the standing-wave design considering mass-transfer effects (nonideal design) are carried out for each splitting strategy. In the nonideal design, the yield is set to 0.95 in each ring for the two sugar products. Product purity, yield, and dilution for each case are obtained from rate model simulations to compare the two different design methods. The total desorbent rate of each splitting strategy is also compared. For this analysis, a system that requires less desorbent and produces a more concentrated product is considered better.

The numerical parameters used in the simulations are listed in Table 9, and the operating parameters (flow rates and switching time) determined from the design methods are listed in Tables 10 and 11. In the simulations, the feed to the second SMB in each strategy is taken as the time-averaged composition of the critical product at steady state; in reality, the product concentration of each component from the first ring can vary periodically even when the system has reached a cyclic steady state (Zhong and Guiochon, 1997; Wu et al., 1998b). After 400 port switchings, the simulated time-averaged concentration of each component at each product port has nearly approached a limiting value. The mass balance is checked for each component over one switching interval. If the difference between the mass introduced and the mass leaving the system through the two product ports for each component during the switching interval is less than 0.5%, then the system is defined here to be at a cyclic steady state.

Figures 3 and 4 show column profiles for two strategies (S1 and S2) to isolate glucose and xylose from a feed mixture that contains both sulfuric acid and acetic acid, via complete separation of the sugars from one acid in each step. Figures 5 and 6 show column profiles of two strategies (S3 and S4) for isolating the two sugars via complete separation from one acid in the first SMB ring and complete separation from the remaining acid in the second ring. The arrows in the figures indicate the standing waves, whereas the stars indicate the pinched waves. The results show that the split of the four

Table 10. Operating Parameters and System Output for Tandem SMB Processes with Complete Separation of All Three Groups of Components

Strategy	S1		S2	
Ring	Ring A	Ring B	Ring A	Ring B
		Ideal Design		
$\delta_{j+1} - \delta_j$	0.326	0.359	0.359	0.326
Column dia. [m]	0.0337	0.0337	0.0337	0.0337
t_s [s]	319.2	159.6	351.6	159.6
F [m^3/s]	5.550×10^{-7}	1.223×10^{-6}	5.550×10^{-7}	1.112×10^{-6}
D [m^3/s]	1.223×10^{-6}	1.338×10^{-6}	1.112×10^{-6}	1.227×10^{-6}
R [m^3/s]	5.550×10^{-7}	1.338×10^{-6}	1.112×10^{-6}	1.112×10^{-6}
E [m^3/s]	1.223×10^{-6}	1.223×10^{-6}	5.550×10^{-7}	1.227×10^{-6}
F^{I} [m^3/s]	2.562×10^{-6}	5.132×10^{-6}	2.328×10^{-6}	3.908×10^{-6}
F^{II} [m^3/s]	1.338×10^{-6}	3.908×10^{-6}	1.773×10^{-6}	2.682×10^{-6}
F^{III} [m^3/s]	1.893×10^{-6}	5.132×10^{-6}	2.328×10^{-6}	3.793×10^{-6}
F^{IV} [m^3/s]	1.338×10^{-6}	3.793×10^{-6}	1.217×10^{-6}	2.682×10^{-6}
Y_1^R	0.96	0.71	**0.99**	0.95
Y_2^R	0.02	**0.93**	**1.00**	0.07
Y_3^R	0.00	**0.93**	**0.98**	0.07
Y_4^R	0.05	0.34	0.23	0.31
Y_1^E	0.04	0.29	0.05	0.05
Y_2^E	**0.97**	0.07	0.00	**0.92**
Y_3^E	**0.99**	0.07	0.03	**0.93**
Y_4^E	**0.95**	0.66	0.76	0.69
C_1^R [kg/m^3]	10.85	0.14	**5.62**	5.34
C_2^R [kg/m^3]	0.19	**3.58**	**4.79**	0.34
C_3^R [kg/m^3]	0.02	**15.55**	**19.82**	1.37
C_4^R [kg/m^3]	0.88	2.23	1.96	0.62
C_1^E [kg/m^3]	0.22	0.06	0.06	0.25
C_2^E [kg/m^3]	**4.20**	0.29	0.08	**4.01**
C_3^E [kg/m^3]	**18.26**	1.26	1.43	**16.67**
C_4^E [kg/m^3]	**7.24**	4.77	12.76	1.22
Purity*	—	0.89	—	0.93
		Nonideal Design		
$\delta_{j+1} - \delta_j$	0.326	0.359	0.359	0.326
Column Dia. [m]	0.0337	0.0660	0.0370	0.0500
t_s [s]	277.2	198.6	226.8	187.2
F [m^3/s]	5.550×10^{-7}	1.895×10^{-6}	5.550×10^{-7}	1.775×10^{-6}
D [m^3/s]	1.988×10^{-6}	8.752×10^{-6}	3.410×10^{-6}	2.953×10^{-6}
R [m^3/s]	6.483×10^{-7}	3.532×10^{-6}	1.775×10^{-6}	2.057×10^{-6}
E [m^3/s]	1.895×10^{-6}	7.113×10^{-6}	2.190×10^{-6}	2.672×10^{-6}
F^{I} [m^3/s]	3.490×10^{-6}	1.985×10^{-5}	5.640×10^{-6}	7.848×10^{-6}
F^{II} [m^3/s]	1.597×10^{-6}	1.274×10^{-6}	3.450×10^{-6}	5.178×10^{-6}
F^{III} [m^3/s]	2.152×10^{-6}	1.463×10^{-5}	4.005×10^{-6}	6.952×10^{-6}
F^{IV} [m^3/s]	1.502×10^{-6}	1.110×10^{-5}	2.230×10^{-6}	4.895×10^{-6}
Y_1^R	0.99 (0.95)	0.67 (—)	**1.00 (0.95)**	0.99 (0.95)
Y_2^R	0.01 (0.05)	**0.99 (0.95)**	**1.00 (0.95)**	0.01 (0.05)
Y_3^R	0.01 (0.05)	**0.99 (0.95)**	**1.00 (0.95)**	0.01 (0.05)
Y_4^R	0.02 (0.05)	0.07 (0.05)	0.05 (0.05)	0.24 (—)
Y_1^E	0.06 (0.05)	0.33 (—)	0.00 (0.05)	0.01 (0.05)
Y_2^E	**0.98 (0.95)**	0.01 (0.05)	0.00 (0.05)	**0.98 (0.95)**
Y_3^E	**0.99 (0.95)**	0.01 (0.05)	0.01 (0.05)	**0.99 (0.95)**
Y_4^E	**0.99 (0.95)**	0.93 (0.95)	0.94 (0.95)	0.77 (—)
C_1^R [kg/m^3]	9.64 (9.21)	0.008 (—)	**3.53 (3.36)**	3.02 (2.89)
C_2^R [kg/m^3]	0.05 (0.41)	**1.46 (1.40)**	**3.01 (2.85)**	0.03 (0.13)
C_3^R [kg/m^3]	0.00 (1.74)	**6.29 (6.01)**	**12.68 (12.09)**	0.12 (0.55)
C_4^R [kg/m^3]	0.24 (0.72)	0.18 (0.13)	0.27 (0.26)	0.06 (—)
C_1^E [kg/m^3]	0.02 (0.17)	0.002 (—)	0.01 (0.14)	0.02 (0.12)
C_2^E [kg/m^3]	**2.75 (2.67)**	0.01 (0.04)	0.01 (0.12)	**1.96 (1.90)**
C_3^E [kg/m^3]	**11.80 (11.32)**	0.04 (0.16)	0.17 (0.52)	**8.31 (8.00)**
C_4^E [kg/m^3]	**4.84 (4.66)**	1.20 (1.23)	4.01 (4.04)	0.14 (—)
Purity*	—	0.98	—	0.98

Note: For all cases, $\epsilon_b = 0.39$, $\epsilon_p = 0.60$, $L_c = 1.0$ m, zone configuration = 3–4–9–4. System output values are from VERSE simulations. Values shown in parentheses represent mass-balance approximations.

*Purity is defined as the fraction (by weight) of the sum of glucose and xylose in the final product.

Table 11. Operating Parameters and System Output for SMB Processes Allowing One Component to Distribute between Two Product Ports

Strategy	S3		S4	
Ring	Ring A	Ring B	Ring A	Ring B
		Ideal Design		
$\delta_{j+1} - \delta_j$	0.326	0.359	0.359	0.326
Column dia. [m]	0.0337	0.0337	0.0337	0.0337
t_s [s]	319.2	318.6	351.6	291.6
F [m^3/s]	5.550×10^{-7}	6.117×10^{-7}	5.550×10^{-7}	6.067×10^{-7}
D [m^3/s]	6.117×10^{-7}	6.700×10^{-7}	6.067×10^{-7}	6.700×10^{-7}
R [m^3/s]	5.550×10^{-7}	6.700×10^{-7}	6.067×10^{-7}	6.067×10^{-7}
E [m^3/s]	6.117×10^{-7}	6.117×10^{-7}	5.550×10^{-7}	6.700×10^{-7}
F^{I} [m^3/s]	1.952×10^{-6}	2.570×10^{-6}	2.328×10^{-6}	2.135×10^{-6}
F^{II} [m^3/s]	1.338×10^{-6}	1.957×10^{-6}	1.773×10^{-6}	1.465×10^{-6}
F^{III} [m^3/s]	1.893×10^{-6}	2.570×10^{-6}	2.328×10^{-6}	2.072×10^{-6}
F^{IV} [m^3/s]	1.338×10^{-6}	1.900×10^{-6}	1.722×10^{-6}	1.465×10^{-6}
Y_1^R	0.96	0.71	0.71	0.96
Y_2^R	0.04	**0.96**	**0.96**	0.05
Y_3^R	0.05	**0.96**	**0.96**	0.05
Y_4^R	0.31	0.23	0.22	0.31
Y_1^E	0.04	0.29	0.29	0.04
Y_2^E	**0.95**	0.04	0.04	**0.95**
Y_3^E	**0.95**	0.04	0.04	**0.95**
Y_4^E	0.69	0.77	0.78	0.69
C_1^R [kg/m^3]	10.86	0.27	7.31	7.01
C_2^R [kg/m^3]	0.40	**7.24**	**8.40**	0.38
C_3^R [kg/m^3]	1.95	**30.66**	**35.68**	1.79
C_4^R [kg/m^3]	5.21	2.19	3.31	1.03
C_1^E [kg/m^3]	0.42	0.12	3.32	0.27
C_2^E [kg/m^3]	**8.28**	0.36	0.39	**7.24**
C_3^E [kg/m^3]	**35.05**	1.57	1.73	**30.67**
C_4^E [kg/m^3]	10.47	8.03	13.07	2.06
Purity*	—	0.94	—	0.94
		Nonideal Design		
$\delta_{j+1} - \delta_j$	0.326	0.359	0.359	0.326
Column Dia. [m]	0.0337	0.0430	0.0370	0.0380
t_s [s]	280.2	214.8	243.0	207.6
F [m^3/s]	5.550×10^{-7}	7.867×10^{-7}	5.550×10^{-7}	9.317×10^{-7}
D [m^3/s]	8.617×10^{-7}	3.318×10^{-6}	2.077×10^{-6}	1.520×10^{-6}
R [m^3/s]	6.300×10^{-7}	1.400×10^{-6}	9.317×10^{-7}	1.073×10^{-6}
E [m^3/s]	7.867×10^{-7}	2.705×10^{-6}	1.700×10^{-6}	1.378×10^{-6}
F^{I} [m^3/s]	2.355×10^{-6}	7.678×10^{-6}	4.948×10^{-6}	4.072×10^{-6}
F^{II} [m^3/s]	1.568×10^{-6}	4.973×10^{-6}	3.248×10^{-6}	2.693×10^{-6}
F^{III} [m^3/s]	2.123×10^{-6}	5.760×10^{-6}	3.803×10^{-6}	3.625×10^{-6}
F^{IV} [m^3/s]	1.493×10^{-6}	4.360×10^{-6}	2.872×10^{-6}	2.552×10^{-6}
Y_1^R	0.99 (0.95)	0.67 (—)	0.67 (—)	0.99 (0.95)
Y_2^R	0.01 (0.05)	**0.99 (0.95)**	**0.99 (0.95)**	0.01 (0.05)
Y_3^R	0.01 (0.05)	**0.99 (0.95)**	**0.99 (0.95)**	0.01 (0.05)
Y_4^R	0.24 (—)	0.06 (0.05)	0.06 (0.05)	0.23 (—)
Y_1^E	0.01 (0.05)	0.33 (—)	0.33 (—)	0.01 (0.05)
Y_2^E	**0.98 (0.95)**	0.01 (0.05)	0.01 (0.05)	**0.98 (0.95)**
Y_3^E	**0.99 (0.95)**	0.01 (0.05)	0.01 (0.05)	**0.99 (0.95)**
Y_4^E	0.76 (—)	0.93 (0.95)	0.94 (0.95)	0.77 (—)
C_1^R [kg/m^3]	9.89 (9.47)	0.03 (—)	4.54 (—)	3.91 (3.74)
C_2^R [kg/m^3]	0.07 (0.42)	**3.71 (3.55)**	**5.66 (5.42)**	0.05 (0.25)
C_3^R [kg/m^3]	0.30 (1.79)	**15.88 (15.17)**	**24.14 (23.03)**	0.21 (1.05)
C_4^R [kg/m^3]	3.60 (—)	0.31 (0.25)	0.55 (0.50)	0.11 (—)
C_1^E [kg/m^3]	0.07 (0.40)	0.01 (—)	1.20 (—)	0.03 (0.15)
C_2^E [kg/m^3]	**6.66 (6.42)**	0.02 (0.10)	0.03 (0.16)	**3.76 (3.64)**
C_3^E [kg/m^3]	**28.42 (27.28)**	0.09 (0.41)	0.13 (0.66)	**16.11 (15.51)**
C_4^E [kg/m^3]	8.98 (—)	2.43 (2.48)	5.14 (5.20)	0.29 (—)
Purity*	—	0.98	—	0.98

Note: For all cases, $\epsilon_b = 0.39$, $\epsilon_p = 0.60$, $L_c = 1.0$ m, zone configuration = 3–4–9–4. System output values are from VERSE simulations. Values shown in parentheses represent mass-balance approximations.

* Purity is defined as the fraction (by weight) of the sum of glucose and xylose in the final product.

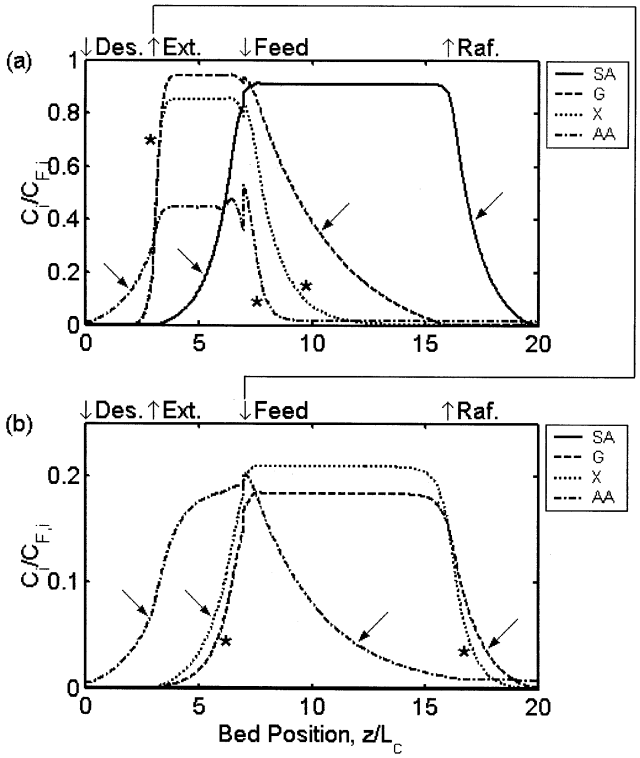

Figure 3. VERSE simulated column profiles for a tandem SMB process for complete separation using Strategy 1 (S1) where sulfuric acid is cleaved first.

(a) Complete separation of glucose (G), xylose (X), and acetic acid (AA) from sulfuric acid (SA). (b) Complete separation of glucose and xylose from acetic acid. Arrows (←): Standing waves. Asterisks (*): pinched waves. Standing waves: zone I*A*, acetic acid; zone II*A*, sulfuric acid; zone III*A*, glucose; zone IV*A*, sulfuric acid; zone I*B*, acetic acid; zone II*B*, xylose; zone III*B*, acetic acid; zone IV*B*, glucose.

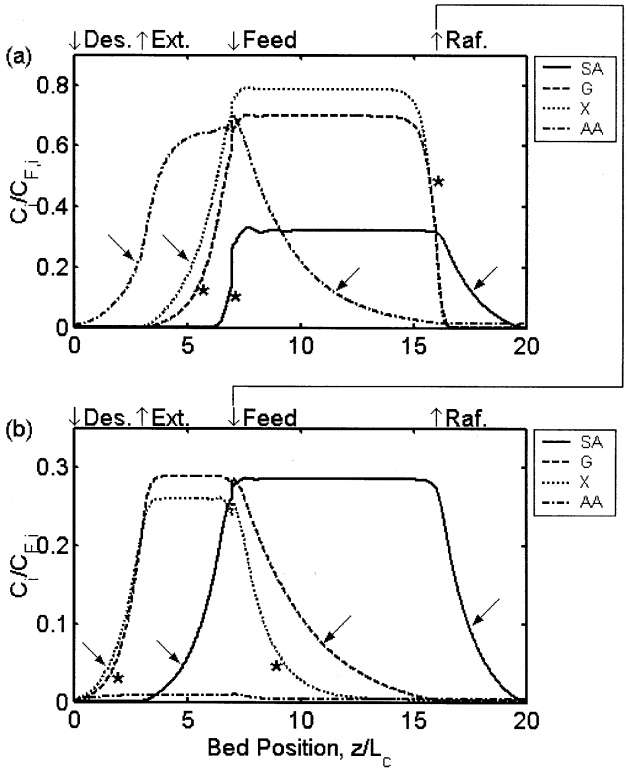

Figure 4. VERSE simulated column profiles for a tandem SMB process for complete separation using Strategy 2 (S2) where acetic acid is cleaved first.

(a) Complete separation of glucose, xylose, and sulfuric acid from acetic acid. (b) Complete separation of glucose and xylose from sulfuric acid. Standing waves: zone I*A*, acetic acid; zone II*A*, xylose; zone III*A*, acetic acid; zone IV*A*, sulfuric acid; zone I*B*, acetic acid; zone II*B*, sulfuric acid; zone III*B*, glucose; zone IV*B*, sulfuric acid.

components in each case follows the intent of the standing-wave design.

The yield, product composition, and final product purity obtained from simulations for each case are summarized in Tables 10 and 11. For each case based on the nonideal design, Tables 10b and 11b show that the simulated product purity is 0.98 for all cases and simulated yield for the sugar product exceeds the target yield, 0.95, in the standing-wave design. The results show that the standing-wave design for nonideal systems can guarantee high product purity and high yield.

Compared to the ideal design (Tables 10a and 11a), the nonideal design (Tables 10b and 11b) for any splitting strategy gives a higher product yield. In addition, the final product purity based on the ideal design ranges from 0.89 to 0.94, which is lower than that of the corresponding nonideal design for all splitting strategies. It is clear from this example that the nonideal design can guarantee high purity and high yield, whereas the ideal design cannot.

Tables 10b and 11b also show a comparison between the mass-balance estimates of product concentrations (numbers in parentheses) and the concentrations obtained from simulations based on the given operating conditions. One can see that the mass-balance approach is generally conservative in that the desired product yields (see bold numbers in Tables 10b and 11b) are underestimated by 3% to 4%. Product concentrations are also underestimated by 3% to 5%. It should be noted in Figures 3 to 4 that within a given zone some waves are not standing, but instead are traveling either faster or slower than the selected standing wave. For example, in Figure 3, the adsorption waves of xylose and acetic acid downstream from the feed port do not migrate as far through that zone as glucose (which is the standing wave there). Xylose and acetic acid are effectively "pinched" toward the feed port because the migration velocities of these solutes are relatively slow. The mass-balance estimates should be used only to obtain a crude estimate of the product composition for a given set of operating parameters.

One can calculate the effective δ for each component from Eqs. 34 and 35 using the operating parameters listed in Tables 10 and 11. The calculated effective δ values indicate that the affinity sequence in each zone remains the same as in the ideal case. In this example, the mass-transfer correction terms do not overtake the equilibrium terms. Therefore, it is expected that the best splitting strategy for a corresponding ideal system, S4, should give the lowest desorbent con-

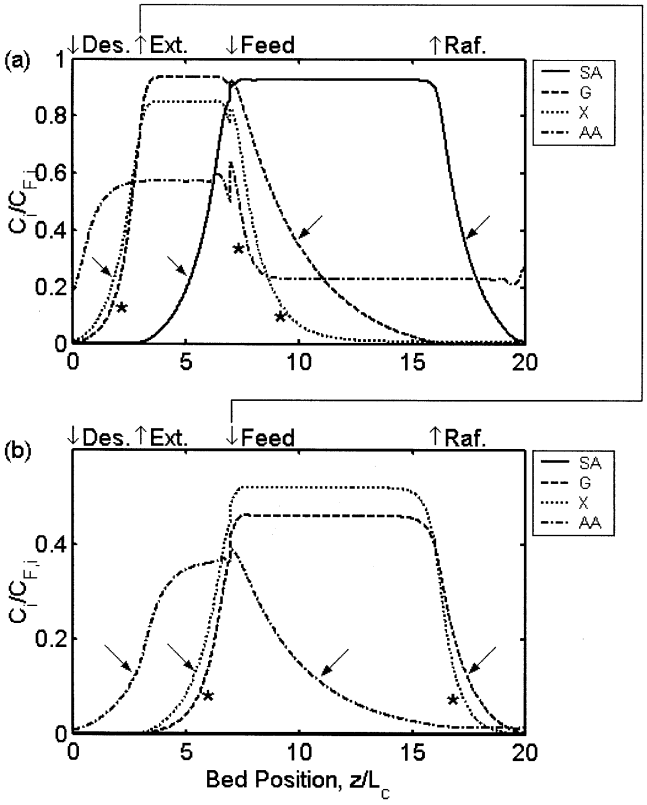

Figure 5. VERSE simulated column profiles for a tandem SMB process for complete separation using Strategy 3 (S3) where acetic acid distributes between two product ports.

(a) Separation of glucose and xylose from sulfuric acid; acetic acid is allowed to distribute between the two product ports. (b) Complete separation of glucose and xylose from acetic acid. Standing waves: zone IA, xylose; zone IIA, sulfuric acid; zone IIIA, glucose; zone IVA, sulfuric acid; zone IB, acetic acid; zone IIB, xylose; zone IIIB, acetic acid; zone IVB, glucose.

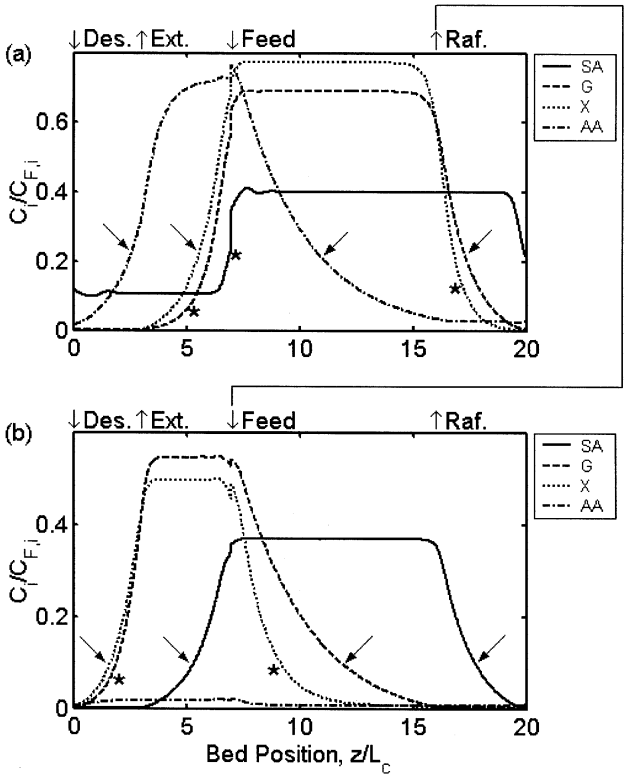

Figure 6. VERSE simulated column profiles for a tandem SMB process for complete separation using Strategy 4 (S4) where sulfuric acid distributes between two product ports.

(a) Separation of glucose and xylose from acetic acid; sulfuric acid is allowed to distribute between the two product ports. (b) Complete separation of glucose and xylose from sulfuric acid. Standing waves: zone IA, acetic acid; zone IIA, xylose; zone IIIA, acetic acid; zone IVA, glucose; zone IB, xylose; zone IIB, sulfuric acid; zone IIIB, glucose; zone IVB, sulfuric acid.

sumption and the highest product concentration for this nonideal system. The results in Table 12 prove that this analysis is valid.

For both ideal and nonideal designs, the strategies with one distributed component (S3 and S4) have lower total desorbent consumption (D_{total}/F) and higher throughput per bed volume than the strategies for complete separation (S3 and S4) (see Table 12). Furthermore, S2, where the easier separation is performed in the first ring, has less desorbent than S1, 8.7% for the ideal design or 37% for the nonideal design. The two strategies with distributed components (S3 and S4) have slightly different desorbent usage for the ideal design (Table 12), because the difference between the δ values of glucose (j_1) and xylose (j_M) is very small. According to the results in Table 4, if δ_{j_i} is the same as δ_{j_M}, the total desorbent usage should be the same. For the nonideal design, S4 (easier separation performed in the first ring) has less desorbent usage than S3 (more difficult separation performed in the first ring). The output of the first ring in S3 is higher than that in S4 at the same feed flow rate (Table 11b). For this reason, the zone linear velocities in the second ring for S3 are higher, resulting in a higher desorbent usage to overcome mass-transfer effects. The difference in the desorbent usage is enhanced by the mass-transfer effects in nonideal systems.

In this example it is assumed that the number of columns, the column length, the zone configuration, and the feed flow rate are fixed in a given SMB unit. In many applications, the equipment has not been built. The column number, diame-

Table 12. Comparison of Splitting Strategies

	F/BV (s^{-1})	D_{total}/F		$(C_{\text{glu,prod}}+C_{\text{xyl,prod}})/(C_{\text{glu,feed}}+C_{\text{xyl,feed}})$	
Strategy	Nonideal	Ideal	Nonideal	Ideal*	Nonideal
S1 (Fig. 3)	6.43×10^{-6}	4.61	19.35	0.38	0.15
S2 (Fig. 4)	9.13×10^{-6}	4.21	11.46	0.41	0.20
S3 (Fig. 5)	1.18×10^{-6}	2.31	7.53	0.75	0.39
S4 (Fig. 6)	1.26×10^{-6}	2.30	6.48	0.75	0.39

Note: Figures 3 to 6 illustrate the column profiles obtained from nonideal design for the sugar acid separation. In each case, the feed flow rate to the first SMB is 5.550×10^{-7} m^3/s.

*The ideal design is applied to the nonideal system, and the results are based on the simulations considering the nonideal effects.

ter, length, and zone configuration can be adjusted to handle any throughput. One could do a systematic search of these parameters that would lead to optimal performance. Notice the ten operating parameters (the four-zone flow rate and step time for each ring) that guarantee desired purity and yield in a tandem SMB can be calculated directly from the standing-wave equations. Therefore, there is no need to find these ten parameters by trial and error or computer simulations. By incorporating the standing-wave equations in an optimization routine, one can focus the search on fewer variables, and, thus, significantly reduce computation time required for optimization.

Conclusions

The standing-wave design methods for linear, ideal, and nonideal systems have been developed to achieve any desired split of three or more components in a single or tandem SMB. Detailed rate-model simulations confirm that the standing-wave design method for nonideal systems guarantees high purity and high yield for the separation of three or more components.

The separation of a mixture with three or more components requires more solvent than does the separation of a binary mixture. When all three products in a ternary mixture need to be recovered in high purity through a tandem SMB, solvent consumption depends not only on the adsorption strengths of the two nearest neighbors, but also those of the most and the least retained components. For ideal systems, the easier separation should be performed in the first ring to achieve low solvent consumption and high product concentration. If only the intermediate component needs to be recovered, it is beneficial to allow one of the two impurities to distribute between the two outlet ports in the first ring. This conclusion also holds for the recovery of a single component or a group of intermediate components from a mixture with more than three components. For nonideal systems, the standing-wave analysis can be used to find the optimal splitting strategies for minimal desorbent consumption (which leads to the highest product concentrations).

A comparison of product compositions calculated from detailed rate model simulations with those calculated from a mass-balance approximation shows that the mass-balance approach gives conservative estimates of product concentrations and product purity. For the example for sugar–acid separation, it underestimates the desired product yields by 3% to 4% and product concentrations by 3% to 5%.

A comparison of the ideal design and nonideal design for the sugar–acid separation shows that mass-transfer effects are not negligible. The ideal design cannot guarantee high-purity and high-yield sugar products.

The standing-wave equations can be easily solved to give the ten operating parameters that guarantee desired purity and yield in a tandem SMB. The equations also can be incorporated in a systematic search routine to find the optimal design for the lowest solvent consumption, the highest throughput, or the lowest purification cost.

Acknowledgments

This study is supported in part by a grant from the Indiana 21st Century Research Technology Fund. The authors are grateful to Dr. Roger D. Whitley of Air Products & Chemicals, Inc., Allentown, PA, for modifying the VERSE simulator to treat dynamic SMB operations in single SMB systems. The authors gratefully acknowledge the U.S. Department of Energy for the experimental SMB data. The authors appreciate helpful discussions with Mr. Sungyong Mun.

Notation

a_i = linear equilibrium distribution coefficient of component i, m^3/m^3 S.V.
c_i = mobile-phase concentration of component i (a function of z and t), kg/m^3
$c_{p,i}$ = pore-phase concentration of component i (a function of r and t), kg/m^3
$C^m_{i,\max}$ = maximum time-averaged concentration of component i in zone m, kg/m^3
$C^m_{i,\min}$ = minimum time-averaged concentration of component i in zone m, kg/m^3
C_i^{DP} = concentration of component i at the desorbent port, kg/m^3
C_i^E = concentration of component i at the extract port, kg/m^3
C_i^F = concentration of component i in the feed solution, kg/m^3
C_i^{FP} = concentration of component i at the feed port, kg/m^3
C_i^R = concentration of component i at the raffinate port, kg/m^3
D = desorbent flow rate, m^3/s
$D_{p,i}$ = intraparticle diffusivity of component i, m^2/s
D_A = desorbent flow rate to ring A in a two-ring SMB, m^3/s
D_B = desorbent flow rate to ring B in a two-ring SMB, m^3/s
D_{total} = total desorbent flow rate to a two-ring SMB, m^3/s
D_i^∞ = Brownian diffusivity of component i, m^2/s
E = extract flow rate, m^3/s
E_A = extract flow rate from ring A in a two-ring SMB, m^3/s
$E^m_{b,i}$ = axial dispersion coefficient of component i in zone m, m^2/s
F = feed flow rate, m^3/s
F^m = flow rate in zone m, m^3/s
F_A = feed flow rate to ring A in a two-ring SMB, m^3/s
F_B = feed flow rate to ring B in a two-ring SMB, m^3/s
i = component index
j = component index, often denoting the desired product
$k^m_{f,i}$ = film mass-transfer coefficient of component i in zone m, m/s
$K_{e,i}$ = size-exclusion coefficient of component i
$K^m_{f,i}$ = lumped mass-transfer coefficient of component i in zone m, s^{-1}
L_c = length of an individual column, m
L^m = length of zone m, m
m = zone number index
n = number of port switches
N = numbering index of highest-affinity component or the number of components
N_c^m = number of columns in zone m
$P \equiv (1-\epsilon_b)/\epsilon_b$ = particle/mobile-fluid volume ratio
P^E = purity of the extract product
P^R = purity of the raffinate product
q_i = solid-phase concentration of component i (a function of r and t), kg/m^3 S.V.
R = raffinate flow rate, m^3/s
R_p = particle radius, m
S = column cross-sectional area, m^2
S.V. = solid volume, m^3
t = time, s

t_p = time required to inject pulse, s
$t_{r,i}$ = retention time of component i, s
t_s = switching time, s
$t_{0,i}$ = elution time of component i neglecting adsorption, s
u_0^m = liquid interstitial velocity in zone m, m/s
V_c = total column volume (particles + voids), m^3
Y_i = yield of component i in its desired product port
z = axial distance along the SMB, m
z_0^m = position of furthest-upstream point in zone m, m
$\aleph$ = set comprising desired components of the extract product
$\Re$ = set comprising desired components of the raffinate product

Greek letters

β_i^m = decay factor of standing wave i in zone m
$\delta_i \equiv K_{e,i}\epsilon_p + (1-\epsilon_p)a_i$ = partition coefficient of component i
Δ_i^m = mass-transfer correction term for standing component i in zone m, m/s
ϵ_b = interparticle void fraction
ϵ_p = intraparticle void fraction
ν = solid movement velocity, m/s
ν_A = solid movement velocity for ring A in a two-ring SMB, m/s
ν_B = solid movement velocity for ring B in a two-ring SMB, m/s

Literature Cited

Ando, M., M. Tanimura, and M. Tamura, "Method of Chromatographic Separation," U.S. Patent No. 4,970,002 (1990).

Azevedo, D. C. S., and A. E. Rodrigues, "Design of a Simulated Moving Bed in the Presence of Mass-Transfer Resistances," *AIChE J.*, **45**, 956 (1999).

Azevedo, D. C. S., and A. E. Rodrigues, "Fructose–Glucose Separation in a SMB Pilot Plant Unit: Modeling Simulation, Design, and Operation," **47**, 2042 (2001).

Baker, J., *Finite Element Computational Fluid Dynamics*, McGraw-Hill, New York (1983).

Berninger, J. A., R. D. Whitley, X. Zhang, and N.-H. L. Wang, "A Versatile Model for Simulation of Reaction and Nonequilibrium Dynamics in Multicomponent Fixed-Bed Adsorption Processes, *Comput. Chem. Eng.*, **15**, 749 (1991).

Biressi, G., O. Ludemann-Hombourger, M. Mazzotti, R.-M. Nicoud, and M. Morbidelli, "Design and Optimisation of a Simulated Moving Bed Unit: Role of Deviations from Equilibrium Theory," *J. Chromatog. A*, **876**, 3 (2000).

Blehaut, J., and R.-M. Nicoud, "Recent Aspects in Simulated Moving Bed," *Analusis*, **26**, M60 (1998).

Broughton, D. B., R. W. Neuzil, J. M. Pharis, and C. S. Brearley, "The Parex Process for Recovering Paraxylene," *Chem. Eng. Prog.*, **66**, 70 (1970).

Chiang, A. S. T., "Complete Separation Conditions for a Local Equilibrium TCC Adsorption Unit," *AIChE J.*, **44**, 332 (1998a).

Chiang, A. S. T., "Continuous Chromatographic Process Based on SMB Technology," *AIChE J.*, **44**, 1930 (1998b).

Ching, C. B., K. H. Chu, K. Hidajat, and M. S. Uddin, "Experimental and Modeling Studies on the Transient Behavior of a Simulated Countercurrent Adsorber," *J. Chem. Eng. Jpn.*, **24**, 614 (1991).

Cussler, E. L., *Diffusion: Mass Transfer in Fluid Systems*, 2nd ed., Cambridge Univ. Press, New York (1997).

Doran, P. M., *Bioprocess Engineering Principles*, Academic Press, San Diego (1995).

Dünnebier, G., J. Fricke, and K.-U. Klatt, "Optimal Design and Operation of Simulated Moving Bed Chromatographic Reactors," *Ind. Eng. Chem. Res.*, **39**, 2290 (2000).

Finlayson, B. A., *Nonlinear Analysis in Chemical Engineering*, McGraw-Hill, New York (1980).

Francotte, E., P. Richert, M. Mazzotti, and M. Morbidelli, "Simulated Moving Bed Chromatographic Resolution of a Chiral Antitussive," *J. Chromatog. A*, **796**, 239 (1998).

Hashimoto, K., S. Adachi, and Y. Shirai, "Continuous Desalting of Proteins with a Simulated Moving-Bed Adsorber," *Agric. Biol. Chem. Tokyo*, **52**, 2161 (1988).

Hashimoto, K., Y. Shirai, and S. Adachi, "A Simulated Moving-Bed Adsorber for the Separation of Tricomponents," *J. Chem. Eng. Jpn.*, **26**, 52 (1993).

Hatanaka, T., and M. Ishida, "A New Process for Multicomponent Continuous Separation by Combining Multiple Liquid Chromatography Columns," *J. Chem. Eng. Jpn.*, **25**, 78 (1992).

Hotier, G., and B. Balannec, "From Batch Elution to Simulated Countercurrent Chromatography," *Rev. Inst. Fr. Petrol.*, **46**, 803 (1991).

Juza, M., M. Mazzotti, and M. Morbidelli, "Simulated Moving-Bed Chromatography and its Application to Chirotechnology," *Trends Biotechnol.*, **18**, 108 (2000).

Kishihara, S., S. Fujii, H. Tamaki, K. B. Kim, N. Wakiuchi, and T. Yamamoto, "Continuous Chromatographic Separation of Sucrose, Glucose and Fructose Using a Simulated Moving-Bed Adsorber," *Int. Sugar J.*, **94**, 305 (1992).

Lielmezs, J., V. Atwal, and H. Aleman, "Magnetic Field Effect on Free Diffusion on Selected Saccharides in Aqueous Solution Through an Inert Porous Membrane," *J. Electrochem. Soc.*, **137**, 3809 (1990).

Ma, Z., and N.-H. L. Wang, "Standing Wave Analysis of SMB Chromatography: Linear Systems," *AIChE J.*, **43**, 2488 (1997).

Ma, Z., R. D. Whitley, and N.-H. L. Wang, "Pore and Surface Diffusion in Multicomponent Adsorption and Liquid Chromatography Systems," *AIChE J.*, **42**, 1244 (1996).

Mallmann, T., B. D. Burris, Z. Ma, and N.-H. L. Wang, "Standing Wave Design of Nonlinear SMB Systems for Fructose Purification," *AIChE J.*, **44**, 2628 (1998).

Masuda, T., T. Sonobe, F. Matsuda, and M. Horie, "Process for Fractional Separation of Multi-Component Fluid Mixture," U.S. Patent No. 5,198,120 (1993).

Mata, V. G., and A. E. Rodrigues, "Separation of Ternary Mixtures by Pseudo-Simulated Moving Bed Chromatography," *J. Chromatog. A*, **939**, 23 (2001).

Mazzotti, M., G. Storti, and M. Morbidelli, "Robust Design of Countercurrent Adsorption Separation Processes: 2. Multicomponent Systems," *AIChE J.*, **40**, 1825 (1994).

Mazzotti, M., R. Baciocchi, G. Storti, and M. Morbidelli, "Vapor-Phase SMB Adsorptive Separation of Linear/Nonlinear Paraffins," *Ind. Eng. Chem. Res.*, **35**, 2313 (1996a).

Mazzotti, M., G. Storti, and M. Morbidelli, "Robust Design of Countercurrent Adsorption Separation: 3. Nonstoichiometric Systems," *AIChE J.*, **42**, 2784 (1996b).

Mazzotti, M., G. Storti, and M. Morbidelli. "Robust Design of Countercurrent Adsorption Separation Processes: 4. Desorbent in the Feed," *AIChE J.*, **43**, 64 (1997).

Migliorini, C., A. Gentilini, M. Mazzotti, and M. Morbidelli, "Design of Simulated Moving Bed Units under Nonideal Conditions," *Ind. Eng. Chem. Res.*, **38**, 2400 (1999).

Migliorini, C. A., M. Mazzotti, and M. Morbidelli, "Design of Simulated Moving Bed Multicomponent Separations: Langmuir Systems," *Sep. Purif. Technol.*, **20**, 79 (2000).

Navarro, A., H. Caruel, L. Rigal, and P. Phemius, "Continuous Chromatographic Separation Process: Simulated Moving Bed Allowing Simultaneous Withdrawal of Three Fractions," *Sep. Purif. Technol.*, **20**, 39 (1997).

Nicolaos, A., L. Muhr, P. Gotteland, R.-M. Nicoud, and M. Bailly, "Application of Equilibrium Theory to Ternary Moving Bed Configurations (Four + Four, Five + Four, Eight and Nine Zones) I. Linear Case," *J. Chromatog. A*, **908**, 71 (2001a).

Nicolaos, A., L. Muhr, P. Gotteland, R.-M. Nicoud, and M. Bailly, "Application of Equilibrium Theory to Ternary Moving Bed Configurations (Four + Four, Five + Four, Eight and Nine Zones) II. Langmuir Case," *J. Chromatog. A*, **908**, 87 (2001b).

Petzold, L. R., "Description of DASSL: A Differential/Algebraic System Solver," Tech. Rep. SAND-82-8637, Lawrence Livermore National Laboratories, CA (1982).

Rhee, H.-K., R. Aris, and N. R. Amundson, "On the Theory of Multicomponent Chromatography," *Philos. Trans. R. Soc. London A*, **267**, 419 (1970).

Rhee, H.-K., R. Aris, and N. R. Amundson, "Multicomponent Adsorption in Continuous Countercurrent Exchangers," *Philos. Trans. R. Soc. London A*, **269**, 187 (1971).
Ruthven, D. M., *Principles of Adsorption and Adsorption Processes*, Wiley-Interscience, New York (1984).
Schulte, M., and J. Strube, "Preparative Enantioseparation by Simulated Moving Bed Chromatography," *J. Chromatog. A*, **906**, 399 (2001).
Storti, G., R. Baciocchi, M. Mazzotti, and M. Morbidelli, "Design of Optimal Operating Conditions of Simulated Moving Bed Adsorptive Separation Units," *Ind. Eng. Chem. Res.*, **34**, 288 (1995).
Storti, G., M. Masi, S. Carrà, and M. Morbidelli, "Optimal Design of Multicomponent Countercurrent Adsorption Separation Processes Involving Nonlinear Equilibria," *Chem. Eng. Sci.*, **44**, 1329 (1989).
Storti, G., M. Mazzotti, M. Morbidelli, and S. Carrà, "Robust Design of Binary Countercurrent Adsorption Separation Processes," *AIChE J.*, **39**, 471 (1993).
Tonkovich, A. L. Y., and R. W. Carr, "Experimental Evaluation of Designs for the Simulated Countercurrent Moving Bed Separator," *AIChE J.*, **42**, 683 (1996).
Villadsen, J. V., and M. L. Michelsen, *Solution of Differential Equation Model by Polynomial Approximation*, Prentice Hall, Englewood Cliffs, NJ (1978).
Whitley, R. D., *Dynamics of Nonlinear Multicomponent Chromatography — Interplay of Mass-Transfer, Intrinsic Sorption Kinetics, and Reaction*, PhD Diss., Purdue Univ., West Lafayette, IN (1990).
Wilson, E. J., and C. J. Geankoplis, "Liquid Mass Transfer at Very Low Reynolds Numbers in Packed Beds," *Ind. Eng. Chem. Fundam.*, **5**, 9 (1966).
Wooley, R., Z. Ma, and N.-H. L. Wang, "A Nine-Zone Simulated Moving Bed for the Recovery of Glucose and Xylose from Biomass Hydrolyzate," *Ind. Eng. Chem. Res.*, **37**, 3699 (1998).
Wu, D.-J., Z. Ma, and N.-H. L. Wang, "Optimization of Throughput and Desorbent in SMB Chromatography for Paclitaxel Purification," *J. Chromatog. A*, **855**, 71 (1999).
Wu, D.-J., R. D. Whitley, Z. Ma, and N.-H. L. Wang, "Mass-Transfer Effects in Dynamic Nonlinear SMB Systems," *Proc. Int. Symp. on Fundamentals of Adsorption*, p. 461 (1998a).
Wu, D.-J., Y. Xie, Z. Ma, and N.-H. L. Wang, "Design of SMB Chromatography for Amino Acid Separations," *Ind. Eng. Chem. Res.*, **37**, 4023 (1998b).
Xie, Y., D.-J. Wu, Z. Ma, and N.-H. L. Wang, "Extended Standing Wave Design Method for Simulated Moving Bed Chromatography: Linear Systems," *Ind. Eng. Chem. Res.*, **39**, 1285 (2000).
Zhong, G., and G. Guiochon, "Analytical Solution for the Linear Ideal Model of Simulated Moving Bed Chromatography," *Chem. Eng. Sci.*, **51**, 4307 (1996).
Zhong, G., and G. Guiochon, "Simulated Moving Bed Chromatography. Effects of Axial Dispersion and Mass Transfer Under Linear Conditions," *Chem. Eng. Sci.*, **52**, 3117 (1997).
Zhong, G., M. S. Smith, and G. Guiochon, "Effect of the Flow Rates in Linear, Ideal, Simulated Moving-Bed Chromatography," *AIChE J.*, **43**, 2960 (1997).

Appendix A: Scheme to Link Decay Coefficients to the Yield of Each Component

To make a design in the presence of mass-transfer resistance (Eqs. 14 to 17 and Eq. 21) it is necessary to specify decay coefficients for the standing concentration waves in each zone. One can specify sufficiently large decay coefficients β_i^m to achieve high purity and high yield (Wu et al., 1998a). However, when zone length and splitting sequence change it can be more convenient to specify β_i^m according to the desired yield of each component. An approach to link the yield of each component, whose concentration wave should be standing, to the values of β_i^m is proposed here.

The approach is based on simple material balances around the inlet and outlet ports. For each component, it is assumed that the concentration profile is flat in a zone in which it is neither standing nor "pinched" (Figure A1). The feed port is treated as a mixing junction between zones II and III and the feed inlet. The desorbent port is treated as a mixing junction between zones I and IV and the desorbent inlet. To use this approach, it is necessary to specify the desired product yield of each component in the mixture (that is, the mass flow rate out of the desired product port divided by the mass flow rate into the feed port at a steady state). This can be denoted by Y_i for each component i. Figure A1 shows schematic column profiles for the standing components in a four-zone SMB. For each component that is required in the raffinate (defined as an element of the set $\mathfrak{R}$), one can write the following four equations

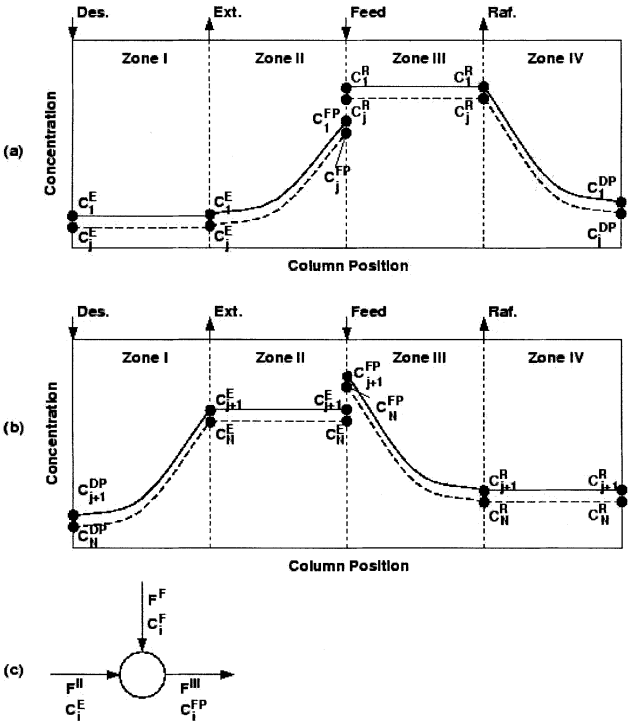

Figure A1. Approximate column profiles for the estimation of product concentrations and β (decay factors).

(a) Column profiles of typical components to be enriched in the raffinate port ($i \in \{1, \ldots, j\}$); (b) column profiles of typical components to be enriched in the extract port ($i \in \{j+1, \ldots, N\}$); (c) mixing junction at the feed port showing how the mass balance is calculated for a component of the extract.

$$C_i^R = \frac{FC_i^F Y_i}{R}, \ \forall i \in \mathfrak{R} \tag{A1}$$

$$C_i^E = \frac{FC_i^F (1-Y_i)}{E}, \ \forall i \in \mathfrak{R} \tag{A2}$$

$$C_i^{FP} = \frac{F^{\mathrm{III}} C_i^R - FC_i^F}{F^{\mathrm{II}}}, \ \forall i \in \mathfrak{R} \tag{A3}$$

$$C_i^{DP} = \frac{F^{\mathrm{I}}}{F^{\mathrm{IV}}} C_i^E, \ \forall i \in \mathfrak{R} \tag{A4}$$

where C_i^R is the time-averaged concentration of component i at the raffinate port, F is the feed flow rate, C_i^F is the concentration of i in the feed solution, C_i^E is the concentration of i in the extract, C_i^{FP} is the concentration of i after the feed port (which is considered to be diluted from the true feed because of the recycle stream from zone II), C_i^{DP} is the concentration of i at the desorbent port, R is the raffinate flow rate, and E is the extract flow rate. For each component i required in the raffinate with specified yield, Eqs. A1–A4 can be solved for C_i^R, C_i^E, C_i^{FP} and C_i^{DP}. Similarly, for each component required in the extract (defined as an element of the set $\aleph$), the concentration at each port can be solved from

$$C_i^R = \frac{FC_i^F(1-Y_i)}{R}, \ \forall i \in \aleph \tag{A5}$$

$$C_i^E = \frac{FC_i^F Y_i}{E}, \ \forall i \in \aleph \tag{A6}$$

$$C_i^{FP} = \frac{F^{\mathrm{II}} C_i^E + FC_i^F}{F^{\mathrm{III}}}, \ \forall i \in \aleph \tag{A7}$$

$$C_i^{DP} = \frac{F^{\mathrm{IV}}}{F^{\mathrm{I}}} C_i^R, \ \forall i \in \aleph \tag{A8}$$

The concentration of each component at each port is in turn used to calculate the decay coefficient for each zone. As an example, an N-component, four-zone SMB for the complete separation of components 1 to j in the raffinate and components $j+1$ to N in the extract would have the following β values

$$\beta_N^{\mathrm{I}} = \ln\left(\frac{C_N^E}{C_N^{DP}}\right) \tag{A9}$$

$$\beta_j^{\mathrm{II}} = \ln\left(\frac{C_j^{FP}}{C_j^E}\right) \tag{A10}$$

$$\beta_{j+1}^{\mathrm{III}} = \ln\left(\frac{C_{j+1}^{FP}}{C_{j+1}^R}\right) \tag{A11}$$

$$\beta_1^{\mathrm{IV}} = \ln\left(\frac{C_1^R}{C_1^{DP}}\right) \tag{A12}$$

Appendix B: Rate Model Equations

The model assumes uniform spherical adsorbent particles, plug flow with constant linear velocity, local equilibrium within the adsorbent, and constant diffusivities. The material balance equation in the bulk fluid phase within each zone includes contributions from convection, axial dispersion, and film mass transfer

$$\frac{\partial c_i}{\partial t} = E_{b,i}^m \frac{\partial^2 c_i}{\partial z^2} - u_0^m \frac{\partial c_i}{\partial z} - \frac{3k_{f,i}^m(1-\epsilon_b)}{R_p \epsilon_b}\left(c_i - c_{p,i}\big|_{r=R_p}\right) \tag{B1}$$

$$z = z_{k,0}, \ E_{b,i}^m \frac{\partial c_i}{\partial z} = u_0^m\left(c_i(t,z_{k,0}) - c_{f,i}(t,z_{k,0})\right) \quad \text{(each column inlet)} \tag{B2}$$

$$z = z_{k,L}, \ \frac{\partial c_i}{\partial z} = 0 \quad \text{(each column outlet)} \tag{B3}$$

$$t = nt_s, \quad c_i = c_i(t, z + L_c) \tag{B4}$$

where c_i is the mobile phase concentration (kg/m^3) of species i at time t (s) and axial position z (m); $c_{f,i}$ represents the inlet concentration of i; m is the zone number (I, II, III, or IV); $E_{b,i}^m$ is the axial dispersion coefficient (m^2/s) of component i in zone m; $z_{k,0}$ represents the axial position of the inlet of column k; $z_{k,L}$ represents the axial position of the outlet of column k; L_c is the length of a single column (m); u_0^m is the mobile phase interstitial velocity (m/s) of zone m; $k_{f,i}^m$ is the film mass-transfer coefficient (m/s); R_p is the particle radius (m); and $c_{p,i}|_{r=R_p}$ is the particle-phase solute concentration at the particle surface (kg/m^3). The numbering of the zones and columns begins at the desorbent port ($z = 0$, $k = 1$, and $m = \mathrm{I}$). The parameter n represents the number of port switches; it can take on integer values between 0 and ∞. The temporal boundary condition, Eq. B4, states that at each switching time the concentration profile is shifted by one column length upstream relative to the direction of liquid flow.

In the pore phase, the material balance equation includes contributions from adsorption and Fickian diffusion

$$K_{e,i}\epsilon_p \frac{\partial c_{p,i}}{\partial t} + (1-\epsilon_p)\frac{\partial q}{\partial t} = K_{e,i}\epsilon_p \frac{D_{p,i}}{r^2}\frac{\partial}{\partial r}\left(r^2 \frac{\partial c_{p,i}}{\partial r}\right) \tag{B5}$$

$$r = 0, \quad \frac{\partial c_{p,i}}{\partial r} = 0 \tag{B6}$$

$$r = R_p, \quad K_{e,i}\epsilon_p D_{p,i}\frac{\partial c_{p,i}}{\partial r} = k_{f,i}^m\left(c_i - c_{p,i}\big|_{r=R_p}\right) \tag{B7}$$

$$t = nt_s, \quad c_{p,i} = c_{p,i}(t,r,z + L_c) \tag{B8}$$

$$t = nt_s, \quad q_i = q_i(t,r,z + L_c) \tag{B9}$$

where $c_{p,i}$ is the pore-phase concentration (kg/m^3); q_i is the solid-phase concentration (kg/m^3 S.V.); r is the distance in the radial direction (m); and $D_{p,i}$ is the intraparticle diffusivity (m^2/s). At $t = 0$, it is assumed that all of the columns are clean, so that $c_{b,i}(0,z) = 0$, $c_{p,i}(0,r,z) = 0$, and $q_i(0,r,z) = 0$.

When the inlet to column k is simply the outlet of column $k-1$, $c_{f,i}(t,z_{k,0}) = c_i(t,z_{k-1,L})$. At the connection points between the zones, we assume zero-volume mixing and enforce the following conditions

$$c_{f,i}(t,z_{k,0}) = \frac{F^{\mathrm{IV}}}{F^{\mathrm{I}}} c_i(t,z_{k-1,L}) \quad \text{zone I inlet; desorbent port} \tag{B10}$$

$$c_{f,i}(t,z_{k,0}) = c_i(t,z_{k-1,L}) \quad \text{zone II inlet; extract port} \tag{B11}$$

$$c_{f,i}(t,z_{k,0}) = \frac{F}{F^{\mathrm{III}}} C_i^F + \frac{F^{\mathrm{II}}}{F^{\mathrm{III}}} c_i(t,z_{k-1,L})$$

zone III inlet; feed port

(B12)

$$c_{f,i}(t,z_{k,0}) = c_i(t,z_{k-1,L}) \qquad \text{zone IV; raffinate port.}$$

(B13)

To solve the column model, the method of orthogonal collocation on finite elements (Villadsen and Michelsen, 1978; Finlayson, 1980; Baker, 1983) is applied. The preceding partial differential equations (Eqs. B1 and B5) are converted to ordinary differential equations (ODEs) through polynomial approximations of the spatial partial derivatives; Legendre polynomials are used in the axial direction and Jacobi polynomials are used in the particle radial direction (Berninger et al., 1991). DASSL (Petzold, 1982), a differential/algebraic system solver, is used to integrate the ODEs in the time domain. The numerical solutions of the governing equations within a single column have been reported previously as the VERSE model (Whitley, 1990; Berninger et al., 1991; Ma et al., 1996).

Manuscript received Aug. 30, 2001, and revision received July 10, 2002.